

RESEARCH ARTICLE

YAP1-mediated regulation of mitochondrial dynamics in IDH1 mutant gliomas

Shruti Patrick¹, Pruthvi Gowda¹, Kirti Lathoria¹, Vaishali Suri² and Ellora Sen^{1,*}

ABSTRACT

Mutation of the isocitrate dehydrogenase 1 (*IDH1*) gene leads to the production of oncometabolite D-2-hydroxyglutarate (2-HG) from α -ketoglutarate and is associated with better prognosis in glioma. As Yes-associated protein 1 (YAP1) is an important regulator of tumor progression, its role in glioma expressing IDH1 with an R132H mutation was investigated. Diminished nuclear levels of YAP1 in IDH1 mutant glioma tissues and cell lines were accompanied by decreased levels of mitochondrial transcription factor A (TFAM). Luciferase reporter assays and chromatin immunoprecipitation were used to investigate the functionality of the TEAD2-binding site on the TFAM promoter in mediating its YAP1-dependent expression. YAP1-dependent mitochondrial fragmentation and ROS generation were accompanied by decreased telomerase reverse transcriptase (TERT) levels and increased mitochondrial TERT localization in IDH1 R132H cells. Treatment with the Src kinase inhibitor bosutinib, which prevents extranuclear shuttling of TERT, further elevated ROS in IDH1 R132H cells and triggered apoptosis. Importantly, bosutinib treatment also increased ROS levels and induced apoptosis in IDH1 wild-type cells when YAP1 was concurrently depleted. These findings highlight the involvement of YAP1 in coupling mitochondrial dysfunction with mitochondrial shuttling of TERT to constitute an essential non-canonical function of YAP1 in the regulation of redox homeostasis.

This article has an associated First Person interview with the first author of the paper.

KEY WORDS: Glioma, IDH1, YAP1, TFAM, TERT, Mitochondria

INTRODUCTION

Somatic mutations in the isocitrate dehydrogenase 1 (*IDH1*) gene are common in low-grade diffuse gliomas and secondary glioblastomas, with point mutation IDH1 R132H being the most prevalent (Parsons et al., 2008). IDH1 R132H is a dominant gain-of-function mutation that causes a shift in substrate specificity, as mutant IDH1 catabolizes α -ketoglutarate to the oncometabolite D-2-hydroxyglutarate (2-HG) in an NADPH-dependent reaction (Bleeker et al., 2010). Consequently, significantly higher levels of 2-HG are found in IDH1 R132H mutant gliomas compared to those in gliomas without the mutation (Dang et al., 2009). This mutation affects various key signaling pathways (Gowda et al., 2018),

including the downregulation of Yes-associated protein 1 (YAP1) and Notch signaling (Wei et al., 2018).

The transcriptional coactivator YAP1 is the main downstream effector of the Hippo signaling pathway, which is involved in tissue growth, repair, regeneration, cell proliferation and apoptosis (Ouyang et al., 2020). The core components of the Hippo pathway, i.e. mammalian serine/threonine kinase 3 and 4 (STK3 and STK4, respectively) and large tumor suppressor kinases 1 and 2 (LATS1 and LATS2, respectively) are involved in phosphorylation, cytoplasmic retention and, ultimately, the proteasomal degradation of YAP1 (Zhao et al., 2010). YAP1 is overexpressed in several solid tumors including gliomas (Orr et al., 2011), and is not only linked to the molecular subtype of gliomas but is also associated with patient prognosis (Guichet et al., 2018). In addition, YAP1 and its downstream signaling pathway Notch is associated with reduced growth of IDH1 mutant astroglial cells (Wei et al., 2018). YAP1 is translocated into the nucleus where it associates with members of the TEA domain-containing transcription factors (TEADs), and YAP1–TEAD complexes regulate genes required for growth and oncogenic transformation (Zhao et al., 2008).

YAP1 is known to regulate mitochondrial structure, function and biogenesis (Mammoto et al., 2018). Mitochondria in cancers have an altered bioenergetic state, and dysregulated mitochondrial metabolism leads to increased levels of mitochondrial reactive oxygen species (ROS) (Wallace, 2012). Transcription factor A, mitochondrial (TFAM) – a nuclear protein essential for packaging, replication and transcription of mitochondrial DNA (mtDNA) – is responsible for its maintenance and biogenesis (Picca and Lezza, 2015). TFAM is upregulated in a number of cancers including gliomas (Hu et al., 2020), and depletion of TFAM is associated with reduced mtDNA copy number, elevated ROS as well as sensitivity to chemotherapeutic drugs (Mei et al., 2015). IDH1 mutant cells, characterized by consumption of NADPH in order to synthesize 2-HG, show decreased levels of reducing power, thereby making them more susceptible to changes in the cellular redox status (Khurshed et al., 2018). IDH1 mutations are also associated with altered mitochondrial function (Li et al., 2015).

mtDNA is highly susceptible to ROS-mediated damage, and is repaired and protected through a number of mechanisms. One such mechanism involves the reversible nuclear exclusion and mitochondrial localization of telomerase reverse transcriptase (TERT) (Ahmed et al., 2008), the enzymatic subunit of the telomerase complex that is responsible for the maintenance of telomeres. TERT is regulated by a number of signaling pathways, one of which is the Hippo/YAP1 pathway (Zhang et al., 2020b), and telomerase activity is associated with the proliferation potential of several malignancies including gliomas (Lee et al., 2017). Telomere dysfunction represses mitochondrial biogenesis, reduces mtDNA content, and decreases mitochondrial mass and energy production (Sahin et al., 2011). Mitochondrial integrity is crucial for cell survival, and TERT binds mtDNA to protect against ROS (Ahmed

¹Division of Cellular and Molecular Neuroscience, National Brain Research Centre, Manesar 122052, India. ²Department of Pathology, All India Institute of Medical Sciences, New Delhi 110029, India.

*Author for correspondence (ellora@nbc.ac.in)

DOI: 10.1242/jcs.259188; S.P., 0000-0003-4007-6547; P.G., 0000-0002-3928-2442; K.L., 0000-0003-0363-399X; V.S., 0000-0001-6485-8194; E.S., 0000-0001-6842-7850

Handling Editor: John Heath

Received 26 July 2021; Accepted 7 October 2021

et al., 2008; Haendeler et al., 2009). Defects in telomeres induced by dysregulated mitochondria are crucial in regulating telomere–mitochondria crosstalk in response to increased mitochondrial ROS levels (Qian et al., 2019), and IDH1 mutation-induced elevation of ROS is associated with increased chemosensitivity of glioma cells (Shi et al., 2015). Besides, IDH1 mutational status (Garrett et al., 2018) and YAP1 expression have been suggested to function as prognostic biomarkers and potential therapeutic targets in gliomas (Guichet et al., 2018). Given that both mitochondrial and telomere functions are crucial for cancer cells (Blasco, 2005; Giampazolias and Tait, 2016); and since YAP1 is known to regulate both mitochondrial function and TERT levels; we decided to evaluate the functional crosstalk between YAP1, TERT and mitochondrial dynamics in gliomas that harbor the IDH1 mutation.

RESULTS

Diminished YAP1 expression in IDH1 R132H cells is C-Jun dependent

As demonstrated previously (Wei et al., 2018), analysis of The Cancer Genome Atlas (TCGA) data shows diminished *YAP1* mRNA levels in gliomas harboring the IDH1 R132H mutation compared with levels in IDH1 wild-type (WT) gliomas (Fig. S1A). A decrease in *YAP1* mRNA (Fig. 1A) and protein levels (Fig. 1B, Fig. S1B) was found in IDH1 R132H cells compared with levels in IDH1 WT cells. A similar decrease in YAP1 protein levels was observed in T98G cells transiently transfected with IDH1 R132H (Fig. S1C). IDH1 mutant cancers are hallmarked by aberrant accumulation of the metabolite 2-HG that mediates many of the phenotypes observed in these cancers. Decreased levels of YAP1 protein were also observed in LN18 cells treated with 2-HG (Fig. 1C, Fig. S1D). Further, immunohistochemical analysis of patient-derived tumor tissue sections showed decreased levels of YAP1 in IDH1 mutant gliomas (Fig. 1D). A similar decrease in YAP1 levels in IDH1 R132H mutant astroglial cells has been reported by Wei et al. (2018).

YAP1 levels are controlled by the Hippo pathway (Dong et al., 2007), and *YAP1* expression is also directly regulated by Wnt/ β -catenin signaling (Konsavage et al., 2012). However, since neither the Hippo pathway nor Wnt signaling are responsible for reduced YAP1 levels in IDH1 R132H cells (Wei et al., 2018), we looked into other potential candidate molecules that function upstream in regulating YAP1. It has been shown that YAP1 expression is dependent on transcription factor C-Jun (Zhang et al., 2020a). TCGA data showed diminished *JUN* mRNA levels in gliomas harboring IDH1 R132H compared with levels in IDH1 WT gliomas (Fig. 1E). A decrease in total C-Jun, as well as in transcriptionally active phosphorylated C-Jun, was seen in IDH1 R132H cells (Fig. 1F, Fig. S1E) and 2-HG treated LN18 cells (Fig. 1G). On further investigation of the status of C-Jun N-terminal kinase (JNK) – the upstream activator of C-Jun, and its active phosphorylated form, no difference between their levels in IDH1 WT and R132H cells was observed (Fig. 1H, Fig. S1F). To confirm the role of C-Jun in regulating the expression of YAP1, we treated IDH1 WT cells that exhibit heightened levels of C-Jun with the JNK inhibitor SP600125 to inhibit phosphorylation and activation of C-Jun. Treatment with SP600125 reduced YAP1 protein levels, suggesting a C-Jun-dependent regulation of YAP1 (Fig. 1I, Fig. S1G).

A diminished amount of YAP1 is accompanied by reduced levels of nuclear TEAD2 in IDH1 R132H cells

Since YAP1 is a transcriptional coactivator that functions within the nucleus, we investigated nuclear YAP1 protein levels in cells.

A decrease in nuclear YAP1 levels was observed in IDH1 R132H cells (Fig. 2A, Fig. S2A) as well as in LN18 cells treated with 2-HG (Fig. 2B, Fig. S2B). Immunohistochemical staining of tissue sections derived from glioma patients showed higher levels of nuclear YAP1 in IDH1 WT gliomas compared with those in IDH1 mutants (Fig. 1D, Fig. 2C).

Members of the TEAD family of transcription factors are crucial for YAP1-mediated gene transcription (Zhao et al., 2008). In the case of IDH1 R132H cells, the decrease in nuclear YAP1 levels was accompanied by reduced nuclear levels of TEAD2 (Fig. 2D, Fig. S2C). LN18 cells treated with 2-HG also showed diminished nuclear TEAD2 levels (Fig. 2E, Fig. S2D). Co-immunoprecipitation showed reduced levels of the YAP1–TEAD2 complex in IDH1 R132H cells as compared to IDH1 WT cells (Fig. S2E). Luciferase reporter assays in IDH1 WT and IDH1 R132H cells transfected with the 8xGTTC construct containing a YAP1-responsive synthetic promoter showed that TEAD-mediated YAP1 activity is diminished in IDH1 R132H cells (Fig. 2F). Analysis of known TEAD target genes using TCGA data further indicated a decrease in YAP1–TEAD transcriptional activity in IDH1 R132H gliomas (Fig. S2F–P).

YAP1–TEAD2 is involved in regulating TFAM expression

YAP1 regulates mitochondrial structure and function (Nagaraj et al., 2012) as well as mitochondrial biogenesis (Mammoto et al., 2018). Since synthesis of mtDNA is essential for mitochondrial biogenesis, we looked into the mtDNA content of IDH1 R132H cells with diminished YAP1 levels. A reduction in mtDNA copy number was observed in IDH1 R132H cells compared to IDH1 WT cells (Fig. 3A). As TFAM regulates mtDNA copy number (Campbell et al., 2012; Ekstrand et al., 2004), and is also necessary for mitochondrial biogenesis and function, its status was investigated in IDH1 R132H cells with reduced YAP1 levels. A decrease in TFAM protein levels was observed in IDH1 R132H cells as compared to IDH1 WT cells, LN18 cells treated with 2-HG (Fig. 3B, Fig. S3A) and T98G cells transiently transfected with IDH1 R132H (Fig. S3B). Immunohistochemical staining of patient-derived tumor tissue sections showed decreased levels of TFAM in IDH1 mutant gliomas when compared with IDH1 WT gliomas (Fig. 3C).

The decrease in TFAM was YAP1 dependent because siRNA-mediated knockdown of YAP1 in IDH1 WT cells diminished TFAM levels, whereas overexpression of YAP1 in IDH1 R132H cells led to an increase (Fig. 3D, Fig. S3C). As a TEAD2-binding site was predicted on the TFAM promoter at position 625–635 using ALGGEN PROMO version 3.0.2 that uses version 8.3 of TRANSFAC (Farre et al., 2003) (Fig. 3E), ChIP was performed to determine whether TEAD2 binding to this site regulates TFAM expression. A higher enrichment of TEAD2 at its predicted binding site on the TFAM promoter was observed in IDH1 WT compared to IDH1 R132H cells, along with higher enrichment of RNA Pol II (Fig. 3E), suggesting that the regulation of TFAM expression by the YAP1–TEAD2 complex. The GAPDH promoter was used as negative control for ChIP.

The dependence of TFAM expression on the YAP1–TEAD2 complex was further confirmed by luciferase reporter assays using constructs containing either the wild-type TFAM promoter (TFAM WT luciferase) or the TFAM promoter with a mutation in the predicted TEAD2 binding site (TFAM Δ luciferase) (Fig. 3F). A decrease in TFAM WT luciferase activity was observed in IDH1 R132H cells compared to IDH1 WT cells transfected with the same construct (Fig. 3G). In addition, compared to the TFAM WT

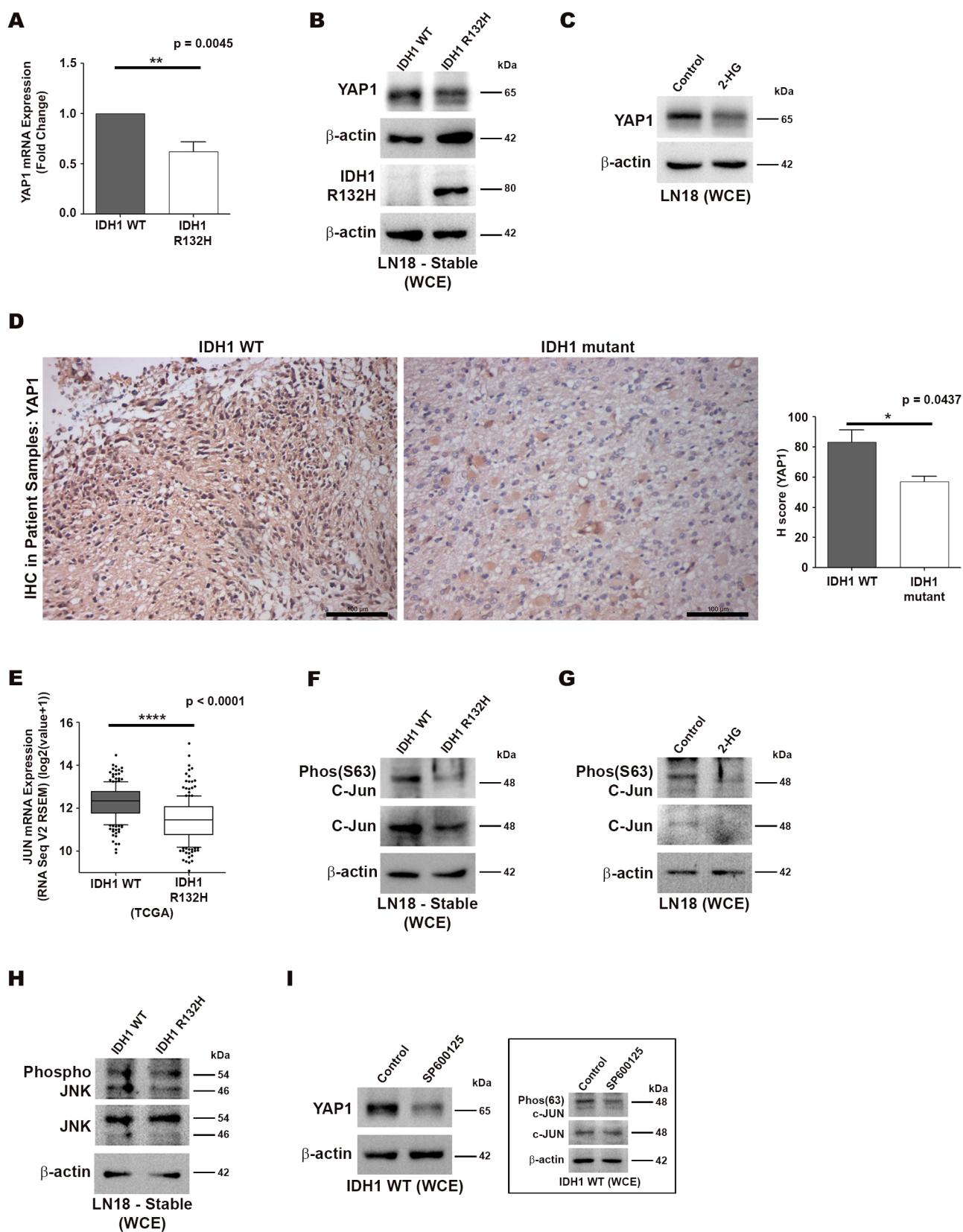


Fig. 1. See next page for legend.

luciferase reporter, the TFAM Δ luciferase reporter showed reduced activity in IDH1 WT cells (Fig. 3H). The role of YAP1 in the expression of TFAM was further validated by using S94A mutant

YAP1, which disrupts its binding to TEAD transcription factors. Although overexpression of wild-type YAP1 in IDH1 R132H cells brought about an increase in TFAM protein levels, there was no

Fig. 1. Reduced YAP1 expression in IDH1 R132H. (A) qRT-PCR reveals reduced YAP1 mRNA levels in IDH1 R132H cells. Data are expressed as fold change over IDH1 WT and presented as mean \pm s.e.m.; $n=5$ biological replicates. $**P<0.01$ (two-tailed Student's t -test). (B) Immunoblots show reduced YAP1 levels in IDH1 R132H cells compared with those in IDH1 WT cells. The expression of mutant IDH1 R132H in the cells is shown. (C) Immunoblots show reduced YAP1 levels in 2-HG-treated LN18 cells. (D) Representative images of patient glioma tissue sections immunohistochemically stained for YAP1 are shown. Scale bars: 100 μ m. Quantitative analysis of IHC images shows increased expression of YAP1 in IDH1 WT tumor tissue compared with that in IDH1 mutants. Data are presented as mean \pm s.e.m. $n=4$ IDH1 WT and $n=3$ IDH1 mutant patients. $*P<0.05$ (two-tailed Student's t -test). (E) TCGA data analysis shows decreased expression of *JUN* mRNA in IDH1 R132H gliomas compared with that in IDH1 WT gliomas. Data from $n=204$ IDH1 WT and 206 IDH1 R132H patients from TCGA have been used for analysis. Whiskers represent 10–90 percentile. $****P<0.0001$ (two-tailed Student's t -test). (F) Immunoblots show reduced levels of total C-Jun and of C-Jun phosphorylated at Ser63 in IDH1 R132H cells compared with those in IDH1 WT cells. (G) Immunoblots show reduced total C-Jun and phosphorylated (Ser63) C-Jun levels in 2-HG-treated LN18 cells. (H) Immunoblots show total and phosphorylated JNK levels in IDH1 WT and IDH1 R132H cells. (I) Immunoblots show reduced levels of YAP1 in IDH1 WT cells on treatment with SP600125. Inset shows reduction in phosphorylated (Ser63) C-Jun levels in SP600125-treated cells. Immunoblots are representative of $n=3$ biological replicates. WCE, whole-cell extract.

such increase on overexpressing YAP1-S94A (Fig. 3I, Fig. S3D). These experiments with TFAM luciferase reporters (TFAM WT or TFAM Δ), together with overexpression of WT or S94A mutant YAP1, demonstrated that the YAP1–TEAD2 interaction is, indeed, involved in regulating TFAM expression.

IDH1 R132H cells show increased mitochondrial fragmentation

The morphology and distribution of the mitochondrial network are maintained through the dynamic balance between fission and fusion, which involves the essential role of mitofusins (Ishihara et al., 2004) and dynamin-related protein 1 (DRP1; also known as DNML) (Imoto et al., 1998), among others. Investigation of mitochondrial morphology using MitoTracker staining showed that mitochondria in IDH1 R132H cells had a more fragmented appearance, while IDH1 WT cells had more fused and branched mitochondria (Fig. 4A). Mitofusin 1 (MFN1) is essential for mitochondrial fusion and maintenance of mitochondrial morphology. Analysis of TCGA data showed decreased expression of *MFN1* mRNA in IDH1 R132H gliomas compared with that in IDH1 WT gliomas (Fig. 4B). Diminished levels of MFN1 were observed in IDH1 R132H cells and in 2-HG-treated LN18 cells (Fig. 4C, Fig. S4A). A similar decrease in MFN1 levels was observed in T98G cells transiently expressing IDH1 R132H (Fig. S4B). MFN1 expression was found to be YAP1 dependent, as knockdown of YAP1 in IDH1 WT cells decreased levels of MFN1 (Fig. 4D, Fig. S4C), whereas YAP1 overexpression in IDH1 R132H cells increased its levels (Fig. 4D, Fig. S4D). In addition to a decrease in MFN1, TCGA data also revealed an increase in *DNM1L* mRNA (which codes for DRP1 protein) levels in IDH1 R132H gliomas (Fig. S4E). Whereas total DRP1 protein levels were found to be lower in IDH1 R132H cells than those in IDH1 WT cells (Fig. S4F), immunoblot analysis of mitochondrial protein fractions showed an increase in DRP1 recruitment to mitochondria in IDH1 R132H cells (Fig. S4G).

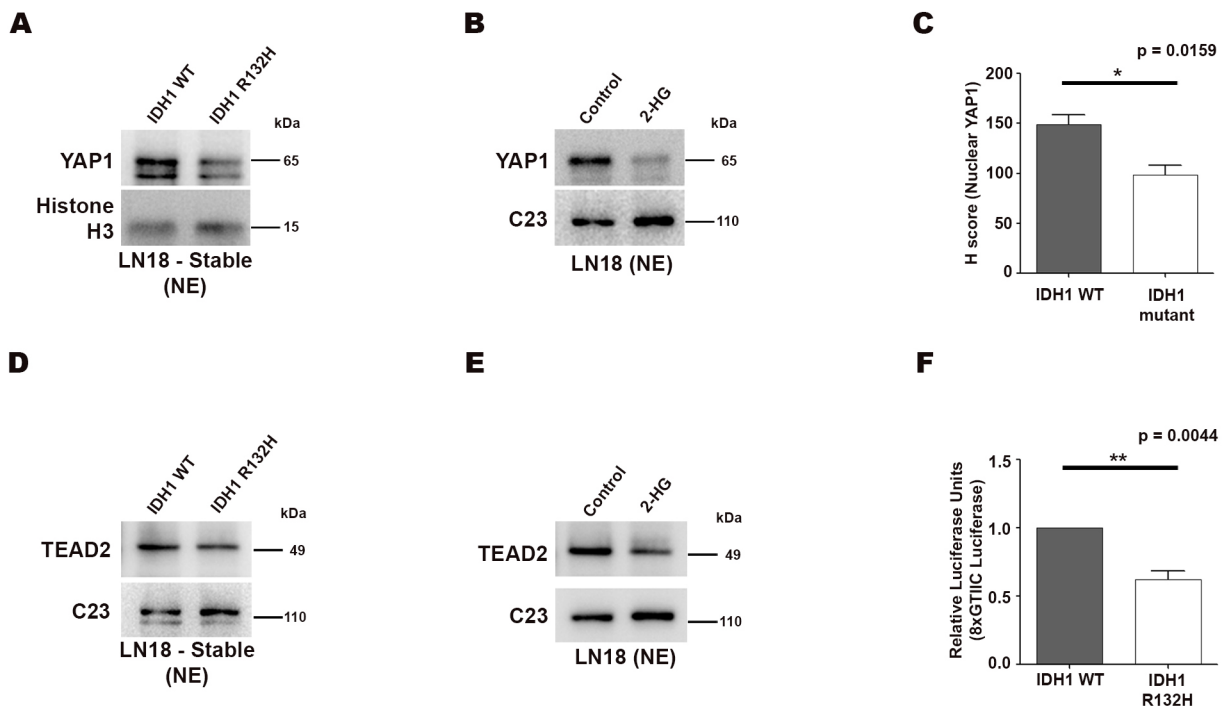


Fig. 2. Reduced nuclear YAP1 and TEAD2 in IDH1 R132H cells. (A) Immunoblots show diminished nuclear YAP1 levels in IDH1 R132H cells compared with those in IDH1 WT cells. (B) Immunoblots show reduced nuclear YAP1 levels in LN18 cells upon treatment with 2-HG. (C) Quantitative analysis of YAP1 IHC staining of glioma tissue sections shows higher levels of nuclear YAP1 in IDH1 WT tumor tissue compared with those in IDH1 mutant tissue. Data are presented as mean \pm s.e.m.; $n=4$ IDH1 WT and $n=3$ IDH1 mutant patients. $*P<0.05$ (two-tailed Student's t -test). (D) Immunoblots show decreased nuclear levels of transcription factor TEAD2 in IDH1 R132H cells. (E) Immunoblots show decreased nuclear levels of TEAD2 in 2-HG-treated LN18 cells. (F) 8xGT1C shows reduced luciferase activity in IDH1 R132H cells compared with that in IDH1 WT cells. Data in relative luciferase units are presented as mean \pm s.e.m.; $n=3$ biological replicates. $**P<0.01$ (two-tailed Student's t -test). Immunoblots are representative of $n=3$ biological replicates ($n=2$ for 2-HG treatment). NE, nuclear extract.

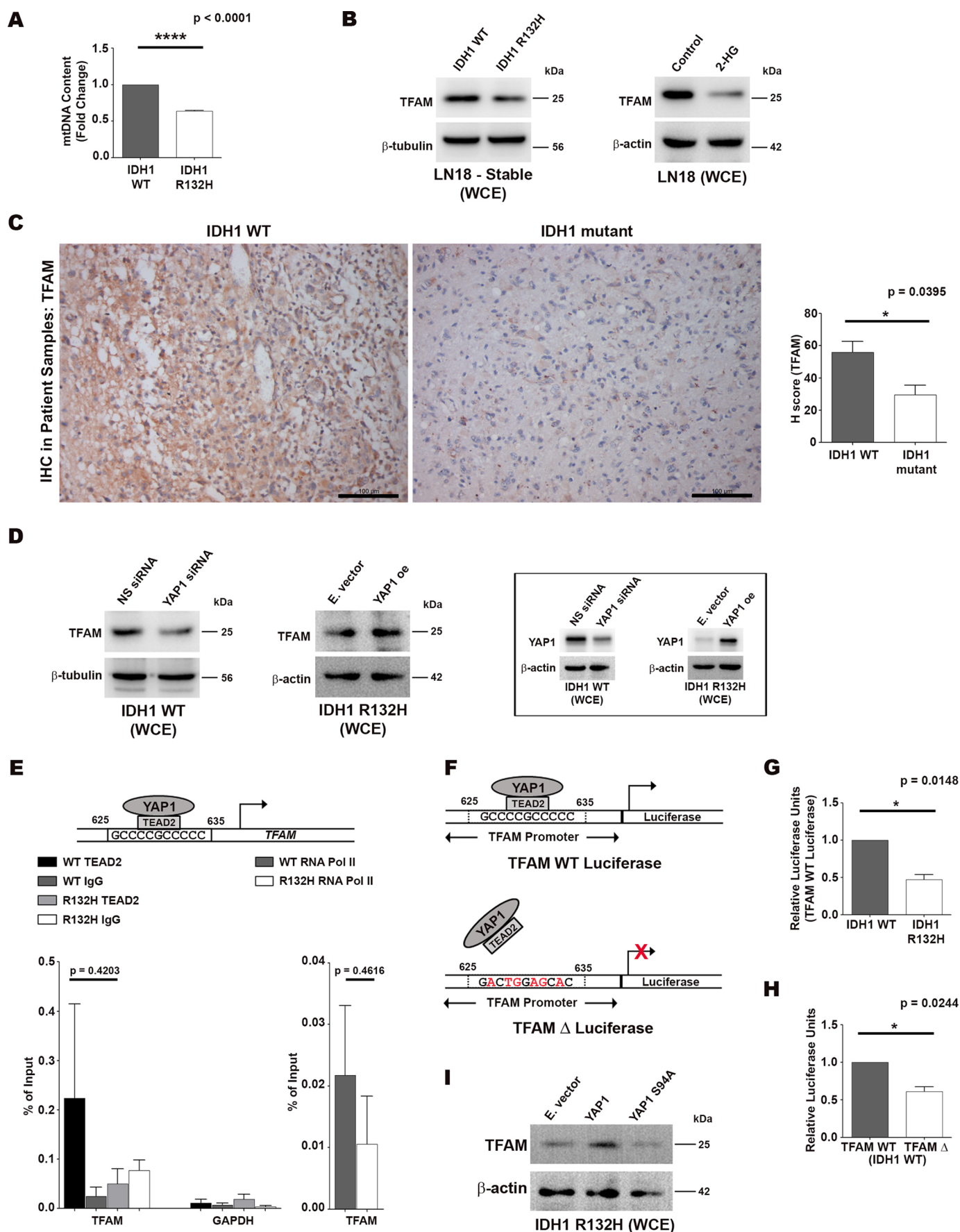


Fig. 3. See next page for legend.

Fig. 3. Regulation of TFAM expression through the YAP1–TEAD2 complex. (A) IDH1 R132H cells show a decrease in mitochondrial DNA (mtDNA) content as determined by qPCR. Data are expressed as fold change over IDH1 WT and presented as mean±s.e.m.; $n=3$ biological replicates. **** $P<0.0001$ (two-tailed Student's t -test). (B). Immunoblots show reduced levels of TFAM in IDH1 R132H cells and 2-HG-treated LN18 cells compared with IDH1 WT and control cells, respectively. (C) Representative images of immunohistochemical staining of glioma tissue sections for TFAM are shown. Scale bars: 100 μ m. Quantitative analysis of IHC images shows higher expression of TFAM in IDH1 WT tumor tissue compared with that in IDH1 mutant tissue. Data are presented as mean±s.e.m.; $n=4$ IDH1 WT and $n=3$ IDH1 mutant patients. * $P<0.05$ (two-tailed Student's t -test). (D) Immunoblots show the reduction in TFAM protein levels upon siRNA-mediated knockdown of YAP1 in IDH1 WT cells, and increase in TFAM levels on overexpressing YAP1 in IDH1 R132H cells. Knockdown and overexpression of YAP1 are shown on the right. (E) Schematic representation of the putative TEAD2-binding site within the TFAM promoter at position 625–635. ChIP-qPCR reveals reduced enrichment of TEAD2 at TFAM promoter in IDH1 R132H compared to IDH1 WT cells. GAPDH promoter is used as negative control. Data are expressed as percentage of input are presented as mean±s.e.m.; $n=3$ biological replicates. P values from two-tailed Student's t -test. (F) Schematic representation of TFAM wild-type (WT) and TFAM mutant (Δ) promoter luciferase constructs. (G) The TFAM WT luciferase construct shows reduced luciferase activity in IDH1 R132H cells compared with that in IDH1 WT cells. Data in relative luciferase units are presented as mean±s.e.m.; $n=2$ biological replicates. * $P<0.05$ (two-tailed Student's t -test). (H) In IDH1 WT cells, the TFAM WT luciferase construct shows higher luciferase activity compared with that shown by the TFAM Δ luciferase construct. Data in relative luciferase units are presented as mean±s.e.m.; $n=2$ biological replicates. * $P<0.05$ (two-tailed Student's t -test). (I) Immunoblots show an increase in TFAM levels upon overexpression of wild-type YAP1 in IDH1 R132H cells but not upon overexpression of S94A mutant YAP1. Immunoblots are representatives of $n=3$ biological replicates. WCE, whole-cell extract; NS siRNA, non-specific siRNA; E. vector, empty vector; YAP1 oe, YAP1 overexpression.

Diminished YAP1 increases mitochondrial fragmentation and ROS accumulation in IDH1 R132H cells

Fragmentation of mitochondria was also found to be dependent on YAP1. siRNA-mediated knockdown of YAP1 in IDH1 WT cells led to increased mitochondrial fragmentation (Fig. 5A), while overexpression of YAP1 in IDH1 R132H cells led to a decrease (Fig. 5B).

As TFAM depletion as well as mitochondrial fission are associated with elevated mitochondrial ROS levels (Woo et al., 2012), the status of ROS in IDH1 R132H cells with diminished TFAM and MFN1 levels was determined. MitoSOX Red staining revealed higher levels of mitochondrial ROS in IDH1 R132H cells compared with those in IDH1 WT cells (Fig. 5C), as well as in LN18 cells treated with 2-HG (Fig. 5D). This increase was YAP1 dependent because siRNA-mediated knockdown of YAP1 led to elevation of mitochondrial ROS in IDH1 WT cells (Fig. 5E), whereas overexpression of YAP1 in IDH1 R132H cells resulted in a reduction in mitochondrial ROS (Fig. 5F).

Increased mitochondrial ROS is concomitant with altered localization and reduced expression of TERT

Given the protective function of TERT in mitochondria under conditions of oxidative stress (Ahmed et al., 2008), we investigated the subcellular localization of TERT in IDH1 R132H cells and in 2-HG-treated LN18 cells exhibiting elevated mitochondrial ROS levels. Immunoblot analysis of mitochondrial and nuclear protein fractions showed an increase in mitochondrial localization of TERT in IDH1 R132H cells compared to that in IDH1 WT cells (Fig. 6A). The extranuclear shuttling of TERT upon 2-HG treatment was reduced on overexpression of YAP1 in 2-HG-treated cells (Fig. 6B).

This reduction in mitochondrial TERT localization was concomitant with diminished ROS levels observed upon YAP1 overexpression (Fig. 5F). The results suggest the involvement of mitochondrial ROS in the translocation of TERT into the mitochondria.

As YAP1 hyperactivation promotes telomerase activity, and increases telomere length and expression of TERT (Zhang et al., 2020b), the status of TERT in IDH1 mutants exhibiting diminished YAP1 was investigated. TCGA data revealed diminished *TERT* mRNA levels in IDH1 R132H gliomas compared with those in IDH1 WT gliomas (Fig. 6C). A decrease in mRNA (Fig. S5A) and protein (Fig. 6D, Fig. S5B) levels of TERT was observed in IDH1 R132H cells. Reduced TERT levels were also found in 2-HG-treated LN18 cells (Fig. 6D, Fig. S5B), and in T98G cells transiently expressing IDH1 R132H (Fig. S5C). Diminished TERT expression in IDH1 R132H cells was accompanied by reduced telomerase activity (Fig. S5D) and decreased telomere length (Fig. S5E). As decrease in nuclear YAP1 was concomitant with diminished TERT expression, the role of YAP1 in the expression of TERT was investigated. Whereas siRNA-mediated knockdown of YAP1 in IDH1 WT cells diminished TERT expression (Fig. 6E, Fig. S5F) and telomerase activity (Fig. S5F), overexpression of YAP1 in IDH1 R132H cells resulted in increased TERT protein levels (Fig. 6E, Fig. S5G) and telomerase activity (Fig. S5G). To corroborate the involvement of YAP1 in regulating the expression of TERT, the YAP1-S94A mutant was employed. Overexpression of wild-type YAP1 in IDH1 R132H cells led to increased TERT levels, but no such increase was seen when YAP1-S94A was overexpressed (Fig. 6F, Fig. S5H). These results suggest that YAP1 regulates TERT expression and that this regulation is TEAD dependent.

YAP1-mediated mitochondrial translocation of TERT affects ROS generation

Mitochondrial localization of TERT protects cells from oxidative stress-induced apoptosis (Miwa et al., 2016). As nuclear exclusion and mitochondrial targeting of TERT are employed by cells under conditions of oxidative stress, we next investigated whether inhibition of TERT translocation to mitochondria affects the generation of ROS, subsequently altering the susceptibility to oxidative stress-mediated death. We treated IDH1 WT and IDH1 R132H cells with the Src kinase inhibitor bosutinib, which blocks TERT nuclear exclusion and mitochondrial localization (Miwa et al., 2016). Whereas bosutinib treatment led to a moderate increase in mitochondrial ROS levels in IDH1 WT cells, it caused a more pronounced elevation of mitochondrial ROS in IDH1 R132H cells (Fig. 7A). Elevation in mitochondrial ROS was also observed upon bosutinib treatment in LN18 cells pretreated with 2-HG (Fig. 7B). Whereas treatment with bosutinib alone was sufficient to considerably raise mitochondrial ROS in IDH1 R132H cells (Fig. 7A), siRNA-mediated knockdown of YAP1 was required in conjunction with bosutinib to bring about a similar increase in ROS levels in IDH1 WT cells (Fig. 7C). Overexpressing YAP1 in IDH1 R132H cells prevented bosutinib treatment-induced increase in mitochondrial ROS levels, thus highlighting the involvement of YAP1 in responsiveness to bosutinib (Fig. 7D). Although cells export TERT to mitochondria under conditions of oxidative stress, the decreased levels of TERT in IDH1 R132H cells dampens their ability to tolerate an increase in ROS generation, thereby rendering these cells more susceptible to agents that block the nuclear export of TERT. This effect of inhibiting the mitochondrial targeting of TERT is evident in IDH1 WT cells when overall TERT levels are lowered upon knockdown of YAP1.

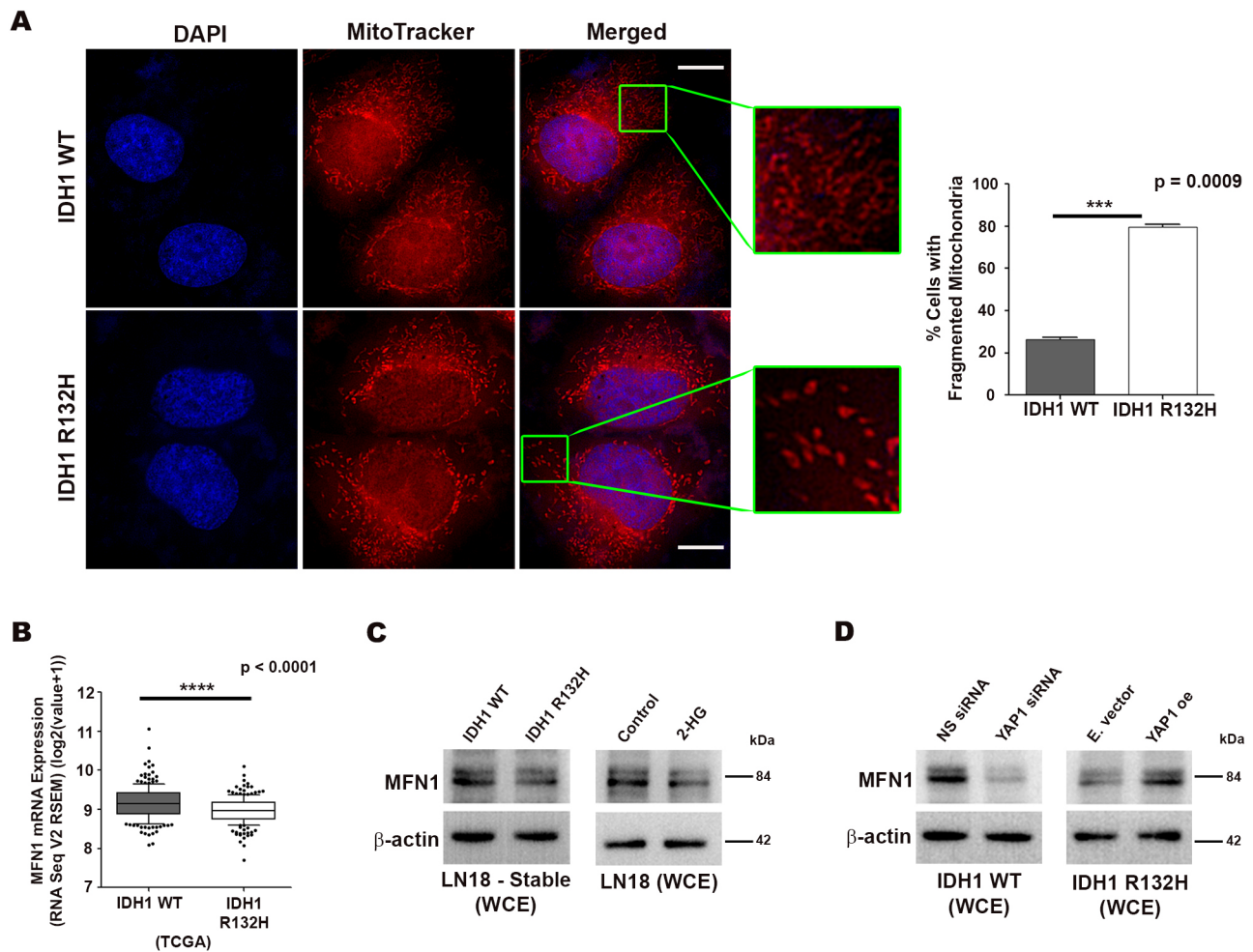


Fig. 4. Increased mitochondrial fragmentation in IDH1 R132H cells. (A) Staining with MitoTracker shows elongated mitochondria in IDH1 WT cells while mitochondria in IDH1 R132H cells have a fragmented morphology. Scale bars: 10 μ m. Graph shows a higher percentage of cells with fragmented mitochondria in the case of IDH1 R132H. Data from ~150 cells under each condition from $n=2$ biological replicates are presented as mean \pm s.e.m.; *** $P<0.001$ (two-tailed Student's t -test). (B) TCGA data analysis shows lower expression of *MFN1* mRNA in IDH1 R132H gliomas compared with that in IDH1 WT gliomas. Data from $n=204$ IDH1 WT and 206 IDH1 R132H patients from TCGA have been used for analysis. Whiskers represent 10–90 percentile. **** $P<0.0001$ (two-tailed Student's t -test). (C) Immunoblots show reduced levels of MFN1 in IDH1 R132H cells and 2-HG-treated LN18 cells compared with those in IDH1 WT and control cells, respectively. (D) Immunoblots show a reduction in MFN1 levels upon siRNA-mediated knockdown of YAP1 in IDH1 WT cells, and increase in MFN1 levels on overexpressing YAP1 in IDH1 R132H cells. Immunoblots are representative of $n=3$ biological replicates. WCE, whole-cell extract; NS siRNA, Non-specific siRNA; E. vector, Empty vector; YAP1 oe, YAP1 overexpression.

Inhibition of extranuclear shuttling of TERT into mitochondria affects apoptotic mediators

We next investigated whether extranuclear shuttling of TERT in IDH1 R132H cells affects survival responses under conditions of elevated oxidative stress. Increased generation of ROS upon inhibition of mitochondrial TERT shuttling in response to treatment with bosutinib was accompanied by increased levels of pro-apoptotic markers, i.e. cleaved caspase 3 (Fig. 7E) and cleaved PARP (Fig. S6B), and an increased BAX to BCL2 ratio (Fig. S6A), TUNEL assays indicated apoptotic cell death in bosutinib-treated IDH1 R132H cells (Fig. 7F, Fig. S6C). The sensitivity of IDH1 R132H-expressing cells to induction of ROS and cell death upon treatment with bosutinib was further confirmed upon treatment with the ROS scavenger N-acetyl-L-cysteine (NAC). Co-treatment with NAC abolished bosutinib-induced death of IDH1 R132H cells (Fig. 7G). In the case of IDH1 WT cells, treatment with bosutinib or YAP1 knockdown alone had some effect in increasing the levels of cleaved caspase 3 and cleaved PARP, and in eliciting apoptotic cell death. However, simultaneous treatment with bosutinib and

knockdown of YAP1 had a synergistic effect on the elevation of cleaved caspase 3 (Fig. 7H), cleaved PARP (Fig. S7B) and BAX versus BCL2 ratio (Fig. S7A). Diminished YAP1 and inhibition of TERT mitochondrial shuttle in IDH1 WT cells triggered apoptosis to levels comparable with bosutinib-treated IDH1 R132H cells (Fig. 7I, Fig. S7C).

DISCUSSION

YAP1 has been shown to regulate several signaling networks that determine the aggressiveness of tumors. YAP1 expression also has a strong correlation with patient survival (Rozengurt et al., 2018). C-Jun, a known upstream regulator of YAP1 (Zhang et al., 2020a), was found to be involved in reducing YAP1 levels in IDH1 R132H cells. TEADs are the main mediators of YAP1 coactivator activity in YAP1-amplified glioblastoma (Stein et al., 2015), and diminished levels of nuclear TEAD2 together with reduced YAP1 levels were crucial in regulating the transcription of TFAM and TERT in IDH1 R132H cells. Also, analysis of TCGA data indicated a significant decrease in the mRNA expression of well-known YAP1–TEAD

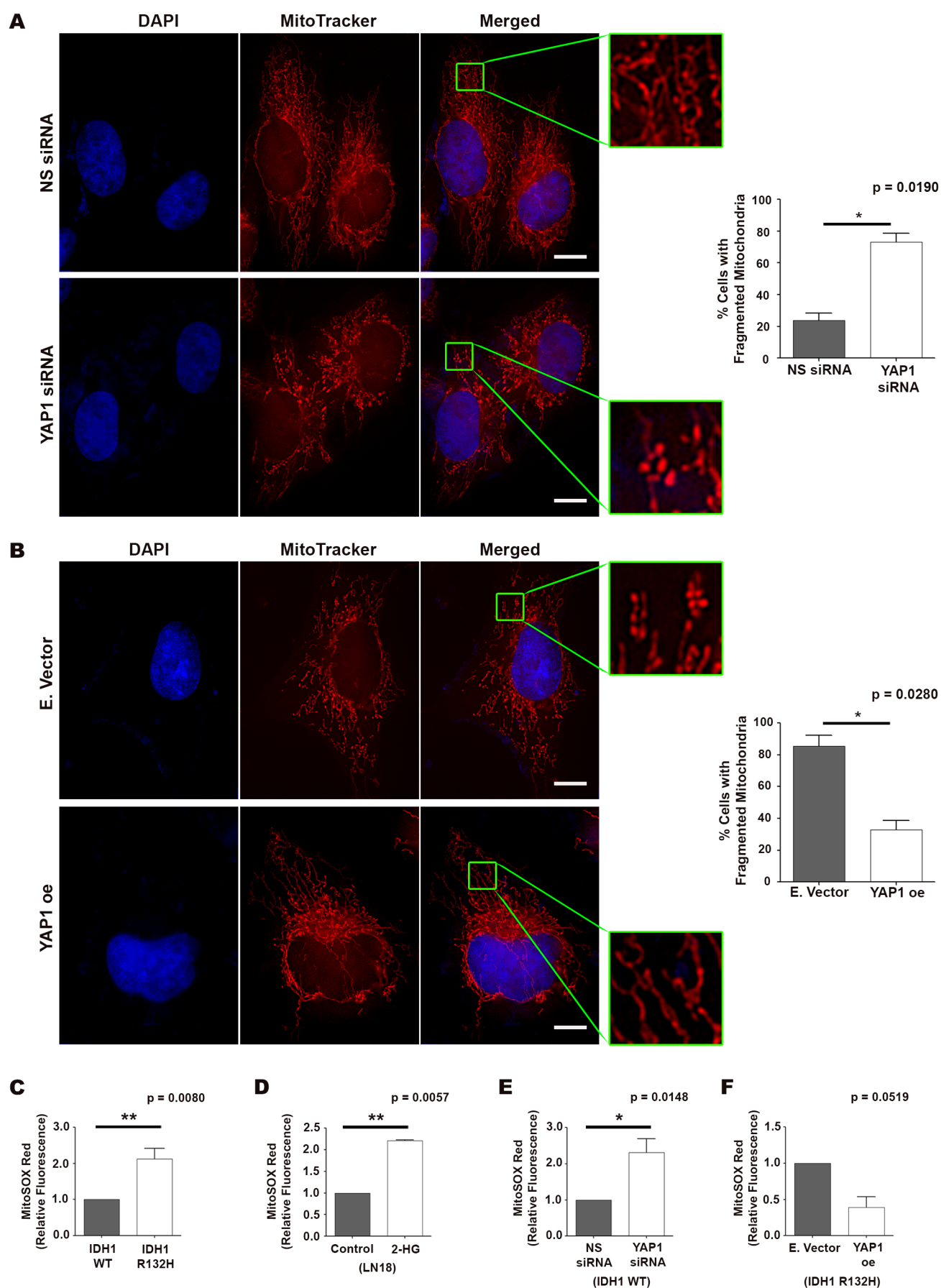


Fig. 5. See next page for legend.

Fig. 5. Role of YAP1 in mitochondrial fragmentation and ROS generation.

(A) Staining with MitoTracker shows elongated mitochondria in IDH1 WT cells transfected with non-specific (NS) siRNA, while mitochondria in IDH1 WT cells transfected with YAP1 siRNA have a more fragmented morphology. Scale bars: 10 μ m. Graph shows a higher percentage of YAP1 siRNA-transfected cells with fragmented mitochondria. Data from ~150 cells under each condition from $n=2$ biological replicates are presented as mean \pm s.e.m.; * $P<0.05$ (two-tailed Student's *t*-test). (B) Staining with MitoTracker shows fragmented mitochondria in IDH1 R132H cells transfected with empty vector (E. Vector), while mitochondria in IDH1 R132H cells overexpressing YAP1 have a more elongated morphology. Scale bars: 10 μ m. Graph shows reduced percentage of YAP1 overexpressing cells with fragmented mitochondria. Data from ~140 cells under each condition from $n=2$ biological replicates are presented as mean \pm s.e.m.; * $P<0.05$ (two-tailed Student's *t*-test). (C) MitoSOX Red staining shows elevated levels of mitochondrial ROS in IDH1 R132H cells. Data are expressed as fold change over IDH1 WT and presented as mean \pm s.e.m.; $n=4$ biological replicates. ** $P<0.01$ (two-tailed Student's *t*-test). (D) MitoSOX Red staining shows increased mitochondrial ROS upon 2-HG treatment in LN18 cells. Data are expressed as fold change over control and presented as mean \pm s.e.m.; $n=2$ biological replicates. ** $P<0.01$ (paired two-tailed Student's *t*-test). (E) siRNA-mediated knockdown of YAP1 leads to an increase in mitochondrial ROS levels in IDH1 WT cells as shown by MitoSOX Red staining. Data are expressed as fold change over non-specific (NS) siRNA-transfected cells and presented as mean \pm s.e.m.; $n=4$ biological replicates. * $P<0.05$ (two-tailed Student's *t*-test). (F) Overexpression of YAP1 leads to a decrease in mitochondrial ROS levels in IDH1 R132H cells as shown by MitoSOX Red staining. Data are expressed as fold change over cells transfected with empty vector and presented as the mean \pm s.e.m.; $n=2$ biological replicates. *P*-value obtained using two-tailed Student's *t*-test.

responsive genes in IDH1 R132H gliomas, suggesting that diminished YAP1–TEAD activity is a feature of IDH1 R132H gliomas. Here, we demonstrate for the first time the involvement of YAP1–TEAD2 in regulating the expression of TFAM. A YAP1-dependent decrease in TFAM was accompanied by reduced MFN1 expression, increased mitochondrial DRP1 levels, and enhanced mitochondrial fragmentation and ROS generation in IDH1 R132H cells. As morphological changes in mitochondria are controlled by their dynamics of fission/fusion, increased recruitment of DRP1 to mitochondria and decreased levels of MFN1 might contribute to enhanced mitochondrial fragmentation in IDH1 R132H cells by favoring fission over fusion. It is likely that the YAP1-mediated decrease of TFAM leads to the subsequent reduction in mitochondrial DNA integrity and heightened mitochondrial ROS in IDH1 mutant glioma.

Diminished levels of TERT under conditions of reduced YAP1 and elevated mitochondrial ROS levels were accompanied by the extranuclear shuttling of TERT into mitochondria. TERT inhibition is regarded as a strategy to facilitate induction of the mitochondrial pathway of apoptosis (Massard et al., 2006). Although mitochondrial TERT localization could contribute to an increased resistance to oxidative stress in IDH1 R132H cells by modulating ROS levels, the concomitant reduction of TERT expression might compensate for this protective role of TERT. Inhibition of mitochondrial TERT shuttling induced death in IDH1 WT cells only under conditions of YAP1 deficiency, a condition that prevails in IDH1 R132H cells to maintain ROS at heightened basal levels. Thus, mitochondrial TERT exerts a protective function against YAP1 deficiency-induced oxidative stress in IDH1 R132H glioma cells and removal of this protection enhances the sensitivity of IDH1 mutant cells to ROS generation.

YAP1 mediates resistance in cancer therapies (Lin et al., 2015), and targeting YAP1 has been suggested as a rationale for potential therapeutic interventions (Liu-Chittenden et al., 2012). Importantly, targeting the YAP–TEAD protein-protein interaction in

glioblastomas with elevated YAP1 expression has been suggested as a viable therapeutic strategy (Saunders et al., 2021). As IDH1 mutations in glioma patients are a predictor of better responsiveness to drug treatments (Hartmann et al., 2011), the ability of diminished YAP1–TEAD2 levels to dampen expression of TERT and TFAM in these patients support the clinical relevance of our findings. Oxidative stress mediates higher chemosensitivity to cisplatin in IDH1 mutant cancer cells compared with that in IDH1 WT cancer cells (Khurshed et al., 2018). Besides, heightened oxidative stress dependent on accumulation of 2-HG in IDH1 mutant cancer cells is associated with increased responsiveness to radiation (Molenaar et al., 2015).

Use of a combination of agents that function synergistically to elevate oxidative stress has been suggested as an efficacious means to inhibit glioma cell growth (Sharma et al., 2007). Bosutinib, a tyrosine kinase inhibitor of the Src/Abl pathway approved for chronic myeloid leukemia, prevents reduction of mitochondrial ROS resulting from TERT accumulation within mitochondria (Miwa et al., 2016). Reduced levels of YAP1 in IDH1 mutant cells determine their resistance to ROS-mediated death stimuli, as bosutinib-induced ROS generation triggered apoptosis in IDH1 WT cells only when YAP1 levels were depleted. Our study not only highlights the non-canonical function of YAP1 in redox regulation but also suggests that the integration of YAP1 inhibitors together with regulators of nuclear-mitochondrial TERT shuttling has important implications for determining the sensitivity of both IDH1 WT and IDH1 R132H cells to ROS stressors. Changes in mitochondrial dynamics and alterations in the redox status modulated by YAP1 in IDH1 wild-type and mutant gliomas might have clinical relevance pertaining to their sensitivity to targeted therapies.

MATERIALS AND METHODS

Cell culture and generation of stable cell lines

Human glioma cell lines LN18 (CRL-2610; ATCC, Manassas, VA) and T98G (CRL-1690; ATCC) were grown in Dulbecco's Modified Eagle Medium (DMEM) (12800; Gibco, Carlsbad, CA) supplemented with 10% heat-inactivated fetal bovine serum (HI-FBS) (10082147; Gibco) and penicillin (100 U/ml)-streptomycin (100 μ g/ml) (15140-122; Gibco). LN18 cells were stably transfected with pEGFP-N1 IDH1 WT and pEGFP-N1 IDH1 R132H constructs (kind gifts from Professor Hai Yan, Duke University School of Medicine, Durham, NC) as described previously (Gowda et al., 2018) to generate stable cell lines, hereafter referred to as IDH1 WT and IDH1 R132H.

Plasmids and site-directed mutagenesis

Cloning and PCR-based mutagenesis was done as described previously (Gowda et al., 2021). TFAM promoter (insert; 803 bp) was cloned into pGL3 basic luciferase reporter vector (E1741; Promega) flanked by MluI and BglII restriction sites. The insert was PCR amplified using One-Step RT-PCR kit (210210; Qiagen). Both the insert and the vector were subjected to restriction digestion using MluI (R0198S; NEB, Ipswich, MA) and BglII (R0144S; NEB) enzymes, ligated overnight using T4 DNA ligase (M0202L; NEB) and transformed into Subcloning Efficiency DH5 α Competent Cells (18265017; Invitrogen). Colonies were screened by PCR and cloning was confirmed by Sanger sequencing. The construct was designated as TFAM WT luciferase.

Mutant plasmids were generated by site-directed mutagenesis. The predicted TEAD2-binding site GCCCGCCCCC in the TFAM WT luciferase construct was mutated to GACTGGAGCAC (mutated residues in bold) by site-directed mutagenesis and PCR with Phusion High-Fidelity DNA Polymerase (M0530S; NEB). The template DNA was eliminated by treatment with DpnI (R0176S; NEB), the product was purified using QIAquick PCR Purification Kit (28104; Qiagen) and transformed into Subcloning Efficiency DH5 α competent cells. Similarly, pBABE YAP1

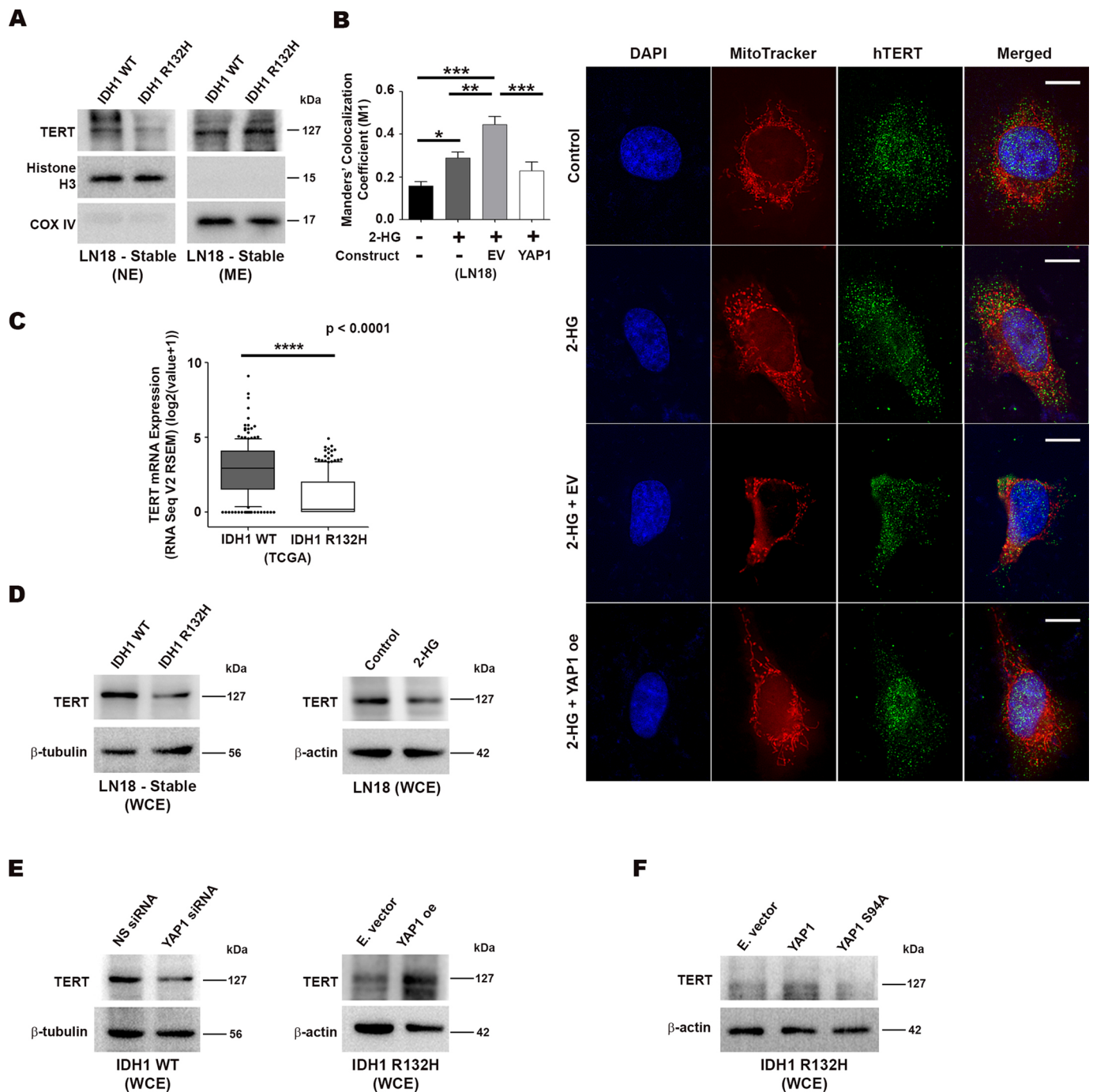


Fig. 6. Altered localization and reduced expression of TERT in IDH1 R132H cells. (A) Immunoblots demonstrating diminished nuclear levels and increased mitochondrial levels of TERT in IDH1 R132H cells. (B) Mitochondrial staining with MitoTracker along with immunostaining shows the localization of TERT under specified conditions. Scale bars: 10 μ m. Graph of Manders' colocalization coefficient (M1) shows an increase in mitochondrial localization of TERT upon treatment with 2-HG. Overexpression of YAP1 in 2-HG-treated cells reduced this mitochondrial localization. Data from 15 cells under each condition from $n=2$ biological replicates are presented as mean \pm s.e.m. Comparisons between groups were done using one-way ANOVA with Tukey's multiple comparison test. * $P<0.05$; ** $P<0.01$; *** $P<0.001$; EV, Empty vector. (C) TCGA data analysis shows lower *TERT* mRNA expression in IDH1 R132H gliomas compared with that in IDH1 WT gliomas. Data from $n=204$ IDH1 WT and 206 IDH1 R132H patients have been used for the analysis. Whiskers represent 10–90 percentile. **** $P<0.0001$ (two-tailed Student's *t*-test). (D) Immunoblots show reduced levels of TERT in IDH1 R132H cells and 2-HG-treated LN18 cells compared with those in IDH1 WT and control cells, respectively. (E) Immunoblots show a reduction in TERT levels upon siRNA-mediated knockdown of YAP1 in IDH1 WT cells, and an increase in TERT levels on overexpressing YAP1 in IDH1 R132H cells. (F) Immunoblots show an increase in TERT levels on overexpression of wild-type YAP1 in IDH1 R132H cells, but not on overexpressing S94A mutant YAP1. Immunoblots are representative of $n=3$ biological replicates ($n=2$ for mitochondrial and nuclear protein fractions). NE, nuclear extract; ME, mitochondrial extract; WCE, whole-cell extract; NS siRNA, non-specific siRNA; E. Vector, empty vector; YAP1 oe, YAP1 overexpression.

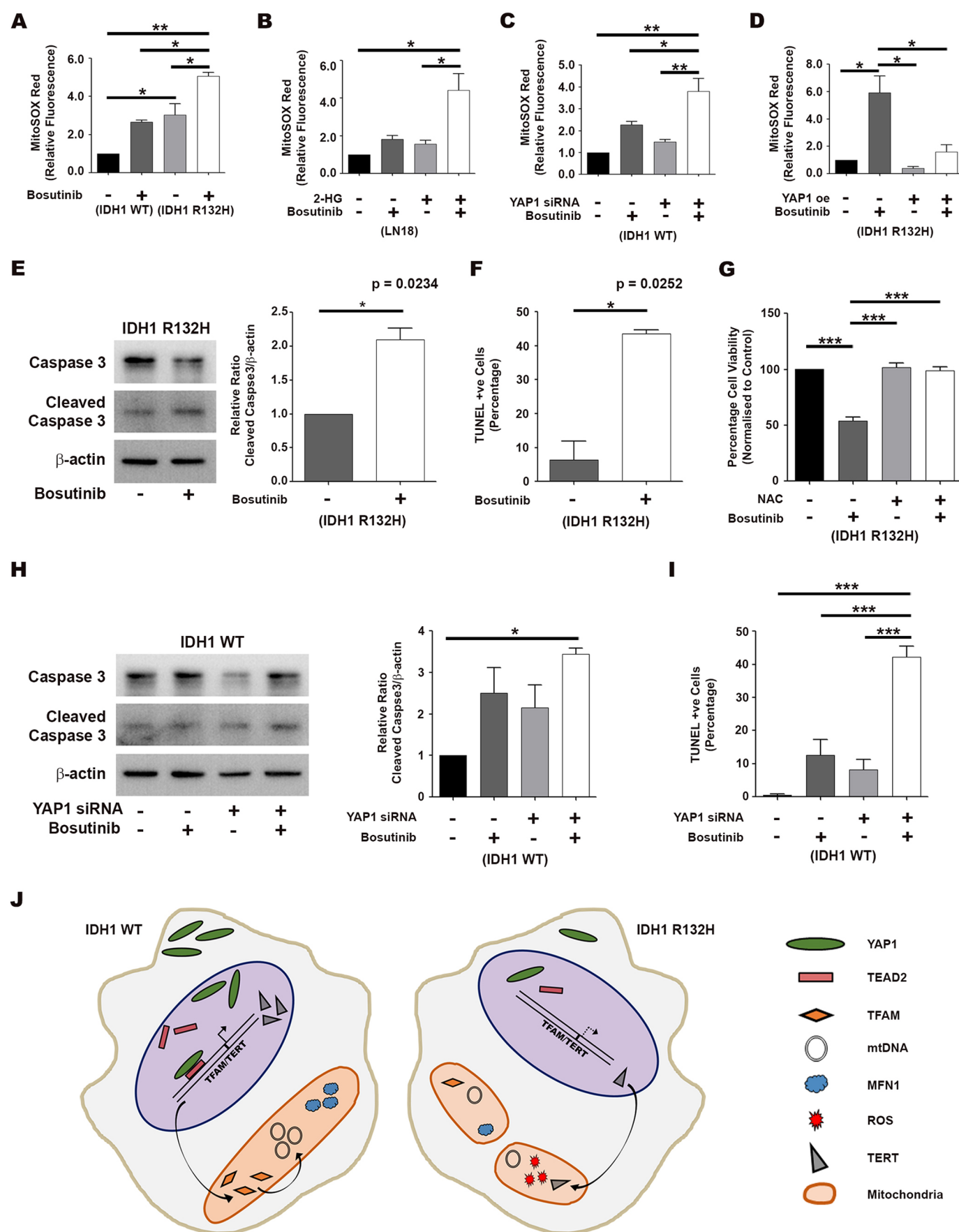


Fig. 7. See next page for legend.

Fig. 7. YAP1-dependent susceptibility to ROS and bosutinib-mediated apoptosis. (A) Upon treatment with bosutinib, MitoSOX Red staining shows a greater elevation of mitochondrial ROS levels in IDH1 R132H cells compared with that in IDH1 WT cells. Data are expressed as fold change over vehicle-treated IDH1 WT cells and presented as mean \pm s.e.m.; $n=2$ biological replicates. (B) Upon treatment with bosutinib, MitoSOX Red staining shows a greater increase of mitochondrial ROS levels in 2-HG-treated cells compared with that in control cells. Data are expressed as fold change over vehicle-treated cells and presented as mean \pm s.e.m.; $n=2$ biological replicates. (C) Treatment of IDH1 WT cells with bosutinib along with siRNA-mediated knockdown of YAP1 has a synergistic effect on the elevation of mitochondrial ROS levels in these cells, as shown by MitoSOX Red staining. Data are expressed as fold change over vehicle-treated, non-specific (NS) siRNA-transfected cells and presented as mean \pm s.e.m.; $n=3$ biological replicates. (D) Overexpression of YAP1 in IDH1 R132H cells prevents elevation in mitochondrial ROS levels in IDH1 R132H cells upon bosutinib treatment, as shown by MitoSOX Red staining. Data are expressed as fold change over vehicle-treated IDH1 R132H cells and presented as mean \pm s.e.m.; $n=2$ biological replicates. (E) Immunoblots show increase in levels of cleaved caspase 3 upon treatment of IDH1 R132H cells with bosutinib. Graph represents cleaved caspase 3 levels expressed as fold change over vehicle control, presented as mean \pm s.e.m.; $n=3$ biological replicates. (F) Treatment with bosutinib leads to apoptotic death of IDH1 R132H cells, as shown by TUNEL assay. Graph represents the percentage of TUNEL-positive cells under each condition, presented as mean \pm s.e.m.; $n=3$ biological replicates. (G) MTS assay shows that treatment with ROS scavenger NAC (N-acetyl-L-cysteine) is sufficient to abrogate bosutinib-mediated death of IDH1 R132H cells. Cell viability is expressed as percentage normalized to control group and presented as mean \pm s.e.m.; $n=3$ biological replicates. (H) Immunoblots show increase in levels of cleaved caspase 3 upon bosutinib treatment along with siRNA-mediated knockdown of YAP1 in IDH1 WT cells. Graph represents cleaved caspase 3 levels expressed as fold change over vehicle-treated, non-specific (NS) siRNA-transfected cells, presented as mean \pm s.e.m.; $n=3$ biological replicates. (I) Treatment of IDH1 WT cells with bosutinib along with siRNA-mediated knockdown of YAP1 leads to apoptotic death as shown by TUNEL assay. Graph represents the percentage of TUNEL-positive cells under each condition, presented as mean \pm s.e.m.; $n=3$ biological replicates. (J) Schematic explaining the role of YAP1 in regulating mitochondrial ROS and TERT-mediated protective effect against oxidative stress in IDH1 WT and IDH1 mutant gliomas. Comparisons between two groups were done using paired two tailed Student's *t*-test. Comparisons among multiple groups were done using one-way ANOVA with Tukey's multiple comparison test. * $P<0.05$; ** $P<0.01$; *** $P<0.001$.

plasmid (Addgene plasmid #15682; Addgene, Watertown, MA) was mutated to replace serine at position 94 with alanine (S94A; by changing TCC to GCG). The mutant constructs were designated TFAM Δ luciferase and pBABE YAP1-S94A, and verified by Sanger sequencing. Primer sequences used for cloning and mutagenesis are provided in Table S1.

Transfections and treatments

T98G, LN18, IDH1 WT and IDH1 R132H cells were seeded into culture dishes 18 h before transfection, and allowed to grow in complete medium (DMEM plus 10% FBS). The medium was replaced with Opti-MEM Reduced Serum Medium (51985034; Gibco) 2 h prior to transfection. Cells were transfected with pBABE-puro (#1764; Addgene), pBABE YAP1 (#15682; Addgene), pBABE YAP1-S94A, pEGFP-N1 IDH1 WT or pEGFP-N1 IDH1 R132H using Lipofectamine 2000 Transfection Reagent (11668-027; Invitrogen), or with 20 nM non-targeting siRNA (D-001210-03-20; Dharmacon, Lafayette, CO) or 75 nM YAP1 siRNA (L-012200-00-0010; Dharmacon) using Lipofectamine RNAiMAX Transfection Reagent (13778-075; Invitrogen). Cells were allowed to grow for 24 h, after which they were either treated further or harvested.

For treatments, the cells were serum-starved for 6 h. Cells were treated with 10 μ M SP600125 (420119; Sigma-Aldrich, St Louis, MO), 40 mM D- α -hydroxyglutaric acid disodium salt (H8378; Sigma-Aldrich) for 48 h, and/or with 5 μ M bosutinib (PZ0192; Sigma-Aldrich) and/or N-acetyl-L-cysteine (NAC) (A9165; Sigma-Aldrich) for 18 h. DMSO (D8418; Sigma-Aldrich) was used as control for bosutinib treatment. Thereafter, the cells were harvested for further processing.

Protein isolation and western blot analyses

Whole-cell and nuclear proteins were extracted from cells as previously described (Gowda et al., 2018). Mitochondria were isolated using the Mitochondrial Isolation Kit for Mammalian Cells (89874; Thermo Scientific, Waltham, MA) by reagent-based method according to manufacturer's instructions. The mitochondrial pellets were resuspended and lysed in mitochondrial lysis buffer containing 50 mM Tris-HCl pH 7.4, 150 mM NaCl, 2 mM EDTA, 2 mM EGTA, 0.2% (v/v) Triton X-100, 0.3% (v/v) NP-40, protease inhibitor cocktail and PMSF to isolate mitochondrial proteins (Arnoult et al., 2009). The nuclear pellets obtained during isolation of mitochondria were resuspended and washed in STM buffer containing 250 mM sucrose, 50 mM Tris-HCl pH 7.4 and 5 mM MgCl₂. Pellets were then resuspended in NET buffer containing 20 mM HEPES pH 7.9, 1.5 mM MgCl₂, 0.5 M NaCl, 0.2 mM EDTA, 20% (v/v) glycerol and 1% (v/v) Triton X-100, incubated on ice for 30 min, sonicated, and centrifuged at 9000 *g* to obtain nuclear protein extract as the supernatant (Dimauro et al., 2012).

Protein concentrations in the various protein extracts were determined using Pierce BCA Protein Assay Kit (23225; Thermo Scientific) according to manufacturer's protocol. Proteins were subjected to electrophoresis and western blot analysis was performed using antibodies against IDH1 R132H (SAB4200548; Sigma-Aldrich), YAP1 (ab52771; Abcam, Cambridge, UK), C-Jun (sc-1694; Santa Cruz Biotechnology, Dallas, TX), C-Jun phosphorylated at Ser63 (9261; Cell Signaling Technologies, Danvers, MA), JNK (9252; Cell Signaling Technologies), phosphorylated JNK (4668; Cell Signaling Technologies), TEAD2 (sc-67115; Santa Cruz Biotechnology), TFAM (NBP1-71648; Novus Biologicals, Littleton, CO), MFN1 (ab57602; Abcam), DRP1 (D6C7; Cell Signaling Technologies), TERT (ab94523; Abcam), Caspase-3 (9662; Cell Signaling Technologies), BAX (sc-493; Santa Cruz Biotechnology) and BCL2 (2872; Cell Signaling Technologies), PARP (9532; Cell Signaling Technologies). Antibodies against β -actin (A3854; Sigma-Aldrich), β -tubulin (sc-9104; Santa Cruz Biotechnology), Histone H3 (9715; Cell Signaling Technologies), C23 (sc-55486; Santa Cruz Biotechnology) or COX-IV (4850; Cell Signaling Technologies) were used to determine equivalent loading. Peroxidase-conjugated secondary antibodies were purchased from Vector Laboratories Inc. (Burlingame, CA). Enhanced chemiluminescence HRP substrate (WBKLS0500; Millipore, Billerica, MA) was added and the blots were imaged using the Syngene G:Box XX8 system (Syngene, Frederick, MD) using GeneSys software (Syngene). Densitometric analyses on the blots were performed using ImageJ. The results were plotted as fold change over control in each case.

Quantitative real-time PCR

Total RNA was isolated from cells using the RNeasy Mini Kit (74104; Qiagen) as per manufacturer's protocol, and cDNA was synthesized using the High-Capacity cDNA Reverse Transcription Kit (4368814; Applied Biosystems Inc., Foster City, CA) on a ProFlex PCR System thermal cycler (Applied Biosystems Inc.). Relative real-time PCR was performed as described previously (Gowda et al., 2018) using Power SYBR Green PCR Master Mix (4367659; Applied Biosystems Inc.) on QuantStudio 5 Real-Time PCR System (Applied Biosystems Inc.). Results were analyzed using the delta delta Ct method and plotted as fold change over control for each transcript. 18S rRNA was used as the internal control. Primer sequences used are listed in Table S1.

Co-immunoprecipitation

Co-immunoprecipitation was performed as previously described (Gowda et al., 2018). Briefly, nuclear protein extracts were incubated with anti-TEAD2 antibody at 4°C for 16 h. This was followed by incubation with protein A/G sepharose beads (6503; Bio Vision, Milpitas, CA) at room temperature for 4 h. The beads were washed with IP buffer, and the immunoprecipitated proteins were subjected to western blot analysis using antibodies against YAP1 and TEAD2. 10% inputs were also processed along with the immunoprecipitated samples.

Chromatin immunoprecipitation

ChIP was performed as described previously (Gowda et al., 2018). Cells were fixed using 1% formaldehyde. Nuclei were isolated and chromatin was

sheared enzymatically using ChIP-IT Express Enzymatic Shearing Kit (53009; Active Motif, Carlsbad, CA). The sheared DNA was immunoprecipitated using anti-TEAD2 or RNA Pol II antibody and protein A/G magnetic beads (6527; Bio Vision). ChIP grade Rabbit IgG (ab171870; Abcam) was used as isotype control. Immunoprecipitated DNA and 10% input samples were purified using phenol-chloroform extraction. Real-time PCR was performed and the results were analyzed by percent input method. Primer sequences used for RT-PCR are given in Table S1.

TRAP assays

Telomeric repeat amplification protocol (TRAP) assays were performed using the TeloTAGGG Telomerase PCR ELISA kit (11854666910; Roche, Basel, Switzerland) as described previously (Ahmad et al., 2016) according to manufacturer's protocol. Briefly, cells were lysed in the lysis reagent and protein concentration in the samples was estimated. From each sample, 0.5 µg of protein was used for the TRAP reaction. Hybridization and ELISA were performed using the PCR product, and absorbance was measured at 450 nm. The relative telomerase activity was determined and expressed as fold change over control.

PCR-based telomere length measurement

Telomere length was measured by quantitative PCR (Cawthon, 2002). DNA was isolated from the cells using QIAamp DNA Mini Kit (51304; Qiagen). 35 ng of DNA was used for each real time PCR reaction, performed using telomere specific primers or primers for single copy gene, *36B4* (*RPLP0*). The average telomere length for each sample was determined indirectly as the T/S ratio, which was calculated as $T/S = [2^{Ct(T)/2^{Ct(S)}}]^{-1} = 2^{-\Delta Ct}$, where, Ct(T) is the Ct value for telomere, Ct(S) is the Ct value for single copy gene *36B4*, and ΔCt is the difference between Ct(T) and Ct(S). The results were expressed as T/S values. Primer sequences used for RT-PCR are given in Table S1.

Quantification of mitochondrial DNA content

Relative mitochondrial DNA content was determined by PCR-based method (Rooney et al., 2015). Total DNA was isolated from the cells using QIAamp DNA Mini Kit (51304; Qiagen) according to manufacturer's protocol, quantified with a spectrophotometer, and diluted to a concentration of 3 ng/µl in TE buffer. Real-time PCR was performed with 6 ng of template DNA using primers for mitochondrial gene *ND1* and nuclear gene *B2M*. Mitochondrial DNA content relative to nuclear DNA content was calculated as $\Delta Ct = Ct(nDNA) - Ct(mtDNA)$ and Relative mtDNA content = $2^{\Delta Ct}$, where, Ct(nDNA) is the Ct value for nuclear gene *B2M* and Ct(mtDNA) is the Ct value for mitochondrial gene *ND1*. The results were expressed as fold change in mtDNA content with respect to control. Primer sequences used for RT-PCR are given in Table S1.

Measurement of mitochondrial ROS

Mitochondrial ROS levels in the cells were measured using MitoSOX Red reagent (M36008; Invitrogen). Cells were grown in 96-well plates. The medium was removed and cells were washed with PBS. This was followed by incubation with 5 µM MitoSOX Red reagent in PBS at 37°C for 25 min. Thereafter, the cells were washed with PBS and fluorescence was measured using Infinite M200 Pro microplate reader (TECAN, Männedorf, Switzerland) (Excitation/Emission: 510/580 nm). The fluorescence intensities were expressed as fold change relative to controls.

MTS assays

Cell viability was determined by MTS assay (G3580; Promega) as described previously (Sheikh et al., 2018). Briefly, cells were grown in 96-well plates and subjected to the required treatments. 20 µl of MTS solution was added to each well. After 4 h of incubation, absorbance was measured at 490 nm. The values were expressed as a percentage relative to control.

Mitochondrial staining and immunofluorescence

Cells grown in chambered glass slides were washed with PBS, and incubated with 20 nM MitoTracker Deep Red FM (M22426; Invitrogen) in phenol-free DMEM at 37°C for 40 min. Cells were then washed with

phenol-free DMEM and fixed with 4% formaldehyde in PBS. Thereafter, the cells were permeabilized with 0.075% Triton X-100 in PBS. For immunostaining, blocking was performed using 2% BSA and 3% serum in PBS. The cells were incubated overnight in primary antibody (TERT; ab94523, Abcam) with 0.1% BSA and 3% serum in PBS at 4°C. This was followed by incubation in secondary antibody (Alexa Fluor 488 – goat anti-rabbit IgG; A11008, Invitrogen) at room temperature for 1.5 h. After staining, cells were mounted in Vectashield Antifade Mounting Medium with DAPI (H-1200; Vector Laboratories Inc.).

TUNEL staining

TUNEL staining was performed using In Situ Cell Death Detection Kit, TMR red (12156792910; Roche) as per manufacturer's instructions. Briefly, cells grown in chambered glass slides were washed with PBS and fixed in 4% formaldehyde in PBS. This was followed by permeabilization using 0.1% Triton X-100 in 0.1% sodium citrate. TUNEL reaction mix containing enzyme solution and label solution was added and cells were incubated at 37°C for 1 h. The slides were washed with PBS and mounted in Vectashield Antifade Mounting Medium with DAPI.

Immunofluorescence and confocal imaging

Mitochondrial staining and immunofluorescence slides were imaged on Nikon Eclipse Ti2 microscope using 100× 1.4 NA oil immersion objective, at a zoom of 1.5, using Andor Zyla sCMOS camera, controlled by NIS-Elements software. Images were acquired at 2560×2160 pixels. TUNEL stained slides were imaged with Nikon A1R confocal microscope configured with Nikon Eclipse Ti2, controlled by NIS-Elements software. Z-stack images of 1024×1024 pixels per frame, with a step size of 1.05 µm, were acquired with 40× 0.95 NA objective, at a scan zoom of 1.241. Line averaging was set to 2 and signals were collected sequentially in two-channel mode.

Image analysis

Widefield fluorescence images were deconvolved on ImageJ using Regularized Inverse Filter algorithm. The mitochondrial morphologies in the cells under each condition were determined based on their appearance by visual inspection. The mitochondria that had a more punctate and disconnected appearance were classified as fragmented, whereas those with a more interconnected and thread-like appearance were classified as not fragmented. The number of cells with fragmented mitochondria were counted and expressed as percentage of total number of cells in each condition. For colocalization analysis, deconvolved widefield fluorescence images were used. ROIs were created around individual cells of interest in the images. Manders' colocalization coefficient (M1) for each ROI was determined using the ImageJ plugin Coloc2.

Confocal images of TUNEL stained slides were used to count the TUNEL-positive cells. The number of TUNEL-positive cells were expressed as percentage of total number of cells in each experimental condition.

Immunohistochemistry

Histologically confirmed IDH1 WT and IDH1 mutant samples of glioblastoma patients were obtained as per the guidelines of the Institutional Human Ethics Committees of All India Institute of Medical Sciences (AIIMS), New Delhi, India and National Brain Research Centre (NBRC), Manesar, India. Formalin fixed paraffin embedded tissue sections were deparaffinized in xylene and rehydrated in graded alcohols. Antigen retrieval was performed in Tris-EDTA-Tween 20 buffer (pH 9.0) for YAP1 and sodium citrate buffer (pH 6.0) for TFAM, at 100°C. Endogenous peroxidase activity was quenched with 1% H₂O₂. The tissues were permeabilized using 0.1% Triton X-100. Blocking was performed in 3% normal goat serum, 1% BSA and 0.05% Triton X-100 for YAP1, and in 3% normal horse serum, 1% BSA and 0.05% Triton X-100 for TFAM. The sections were incubated in rabbit monoclonal antibody to YAP1 (1:50; overnight) or mouse monoclonal antibody to TFAM (1:60; 48 h) at 4°C in a humidified chamber. This was followed by washes with TBS (YAP1) or PBS (TFAM) after which, the sections were incubated with biotinylated anti-rabbit or anti-mouse secondary antibodies for YAP1 and TFAM,

respectively, at room temperature in a humidified chamber. Thereafter, the sections were processed with VECTASTAIN Elite ABC-HRP kit (PK-6100; Vector Laboratories Inc.) for YAP1 or with streptavidin HRP (SA50054; Vector Laboratories Inc.) for TFAM, counterstained with hematoxylin, dehydrated in graded alcohols, cleared in xylene and mounted in DPX.

IHC imaging and analysis

Images were captured with Leica DMRXA2 microscope using Leica Application Suite software. Representative images of four IDH1 WT tumors and three IDH1 mutant tumors each were used for quantitative evaluation of IHC signals of YAP1 and TFAM. Quantification was performed in an automated manner using IHC profiler plugin for ImageJ (Varghese et al., 2014). Staining intensities in the images were divided into four categories by the plugin as: 0, negative staining; 1, low positive staining; 2, positive staining and, 3, high positive staining. H-scores were calculated as $(3 \times \% \text{ of high positive}) + (2 \times \% \text{ of positive}) + (1 \times \% \text{ of low positive})$.

Promoter luciferase reporter assays

Luciferase reporter assays were performed using cells transfected with different combinations of plasmids. IDH1 WT and IDH1 R132H cells were grown in 24-well culture plates, and transfected with 500 ng of 8xGTIC construct (#34615; Addgene) using Lipofectamine 2000 Transfection Reagent, or 500 ng TFAM WT or TFAM Δ luciferase constructs using Lipofectamine 3000 Reagent (L3000015; Invitrogen) along with 20 ng of Renilla luciferase vector, pRL-TK (E2241; Promega) for normalization of transfection efficiency. Cells were lysed and analysed using the Dual-Luciferase Reporter Assay System (E1960; Promega) on GloMax Explorer Multimode Microplate Reader (Promega).

TCGA data analysis

The Cancer Genome Atlas (TCGA) data for mRNA expression (RNA Seq V2 RSEM) of genes of interest from low-grade glioma (LGG) and glioblastoma (GBM) datasets were downloaded from the cBioPortal for Cancer Genomics. Data were segregated based on the IDH1 mutational status (IDH1 WT and IDH1 R132H), log transformed and compared by using unpaired two-tailed Student's *t*-test.

Statistical analysis

Statistical analysis was performed using GraphPad Prism. Data are represented as the mean \pm s.e.m. Comparisons between two groups were carried out using two-tailed Student's *t*-test, unless otherwise indicated. Comparisons among multiple groups were carried out using one-way ANOVA with Tukey's multiple comparison test. Statistical significance is indicated as **P*<0.05; ***P*<0.01; ****P*<0.001 and *****P*<0.0001.

Acknowledgements

We acknowledge Shanker Datt Joshi for help with immunohistochemistry and Rajesh Kumar Kumawat for technical assistance. We are thankful for reagents and antibodies provided by Dr Rajender Motiani (Regional Centre for Biotechnology, Faridabad) and Dr Pankaj Seth (National Brain Research Centre, Manesar).

Competing interests

The authors declare no competing or financial interests.

Author contributions

Conceptualization: S.P., E.S.; Validation: S.P., P.G., K.L.; Formal analysis: S.P.; Investigation: S.P., P.G., K.L.; Resources: V.S., E.S.; Writing - original draft: S.P., E.S.; Writing - review & editing: S.P., P.G., K.L., E.S.; Visualization: S.P., E.S.; Supervision: E.S.; Project administration: E.S.; Funding acquisition: E.S.

Funding

This work was supported by a research grant from the Department of Biotechnology (DBT) (Government of India grant number: BT/Med/30/SP11016/2015) to E.S.

References

Ahmad, F., Dixit, D., Sharma, V., Kumar, A., Joshi, S. D., Sarkar, C. and Sen, E. (2016). Nrf2-driven TERT regulates pentose phosphate pathway in glioblastoma. *Cell Death Dis.* **7**, e2213. doi:10.1038/cddis.2016.117

- Ahmed, S., Passos, J. F., Birket, M. J., Beckmann, T., Brings, S., Peters, H., Birch-Machin, M. A., Von Zglinicki, T. and Saretzki, G. (2008). Telomerase does not counteract telomere shortening but protects mitochondrial function under oxidative stress. *J. Cell Sci.* **121**, 1046-1053. doi:10.1242/jcs.019372
- Arnoult, D., Soares, F., Tattoli, I., Castanier, C., Philpott, D. J. and Girardin, S. E. (2009). An N-terminal addressing sequence targets NLRX1 to the mitochondrial matrix. *J. Cell Sci.* **122**, 3161-3168. doi:10.1242/jcs.051193
- Blasco, M. A. (2005). Telomeres and human disease: ageing, cancer and beyond. *Nat. Rev. Genet.* **6**, 611-622. doi:10.1038/nrg1656
- Bleeker, F. E., Atai, N. A., Lamba, S., Jonker, A., Rijkeboer, D., Bosch, K. S., Tigchelaar, W., Troost, D., Vandertop, W. P., Bardelli, A. et al. (2010). The prognostic IDH1(R132) mutation is associated with reduced NADP+-dependent IDH activity in glioblastoma. *Acta Neuropathol.* **119**, 487-494.
- Campbell, C. T., Kolesar, J. E. and Kaufman, B. A. (2012). Mitochondrial transcription factor A regulates mitochondrial transcription initiation, DNA packaging, and genome copy number. *Biochim. Biophys. Acta* **1819**, 921-929.
- Cawthon, R. M. (2002). Telomere measurement by quantitative PCR. *Nucleic Acids Res.* **30**, e47. doi:10.1093/nar/30.10.e47
- Dang, L., White, D. W., Gross, S., Bennett, B. D., Bittinger, M. A., Driggers, E. M., Fantin, V. R., Jang, H. G., Jin, S., Keenan, M. C. et al. (2009). Cancer-associated IDH1 mutations produce 2-hydroxyglutarate. *Nature* **462**, 739-744. doi:10.1038/nature08617
- Dimauro, I., Pearson, T., Caporossi, D. and Jackson, M. J. (2012). A simple protocol for the subcellular fractionation of skeletal muscle cells and tissue. *BMC Res Notes* **5**, 513. doi:10.1186/1756-0500-5-513
- Dong, J., Feldmann, G., Huang, J., Wu, S., Zhang, N., Comerford, S. A., Gayyed, M. F., Anders, R. A., Maitra, A. and Pan, D. (2007). Elucidation of a universal size-control mechanism in Drosophila and mammals. *Cell* **130**, 1120-1133. doi:10.1016/j.cell.2007.07.019
- Ekstrand, M. I., Falkenberg, M., Rantanen, A., Park, C. B., Gaspari, M., Hultenby, K., Rustin, P., Gustafsson, C. M. and Larsson, N. G. (2004). Mitochondrial transcription factor A regulates mtDNA copy number in mammals. *Hum. Mol. Genet.* **13**, 935-944. doi:10.1093/hmg/ddh109
- Farre, D., Roset, R., Huerta, M., Adsuara, J. E., Rosello, L., Alba, M. M. and Messegue, X. (2003). Identification of patterns in biological sequences at the ALGEN server: PROMO and MALGEN. *Nucleic Acids Res.* **31**, 3651-3653. doi:10.1093/nar/gkg605
- Garrett, M., Sperry, J., Braas, D., Yan, W., Le, T. M., Mottahedeh, J., Ludwig, K., Eskin, A., Qin, Y., Levy, R. et al. (2018). Metabolic characterization of isocitrate dehydrogenase (IDH) mutant and IDH wildtype gliomaspheres uncovers cell type-specific vulnerabilities. *Cancer Metab.* **6**, 4. doi:10.1186/s40170-018-0177-4
- Giampanzolis, E. and Tait, S. W. (2016). Mitochondria and the hallmarks of cancer. *FEBS J.* **283**, 803-814. doi:10.1111/febs.13603
- Gowda, P., Patrick, S., Singh, A., Sheikh, T. and Sen, E. (2018). Mutant isocitrate dehydrogenase 1 Disrupts PKM2-beta-Catenin-BRG1 transcriptional network-driven CD47 expression. *Mol. Cell. Biol.* **38**, e00001-18. doi:10.1128/MCB.00001-18
- Gowda, P., Lathoria, K., Sharma, S., Patrick, S., Umdor, S. B. and Sen, E. (2021). Rewiring of lactate-IL-1beta auto-regulatory loop with Clock-Bmal1: A feed-forward circuit in glioma. *Mol. Cell. Biol.* **41**, e00449-20. doi:10.1128/MCB.00449-20
- Guichet, P. O., Masliantsev, K., Tachon, G., Petropoulos, C., Godet, J., Larrieu, D., Milin, S., Wager, M. and Karayan-Tapon, L. (2018). Fatal correlation between YAP1 expression and glioma aggressiveness: clinical and molecular evidence. *J. Pathol.* **246**, 205-216. doi:10.1002/path.5133
- Haendeler, J., Drose, S., Buchner, N., Jakob, S., Altschmied, J., Goy, C., Spyridopoulos, I., Zeiher, A. M., Brandt, U. and Dimmeler, S. (2009). Mitochondrial telomerase reverse transcriptase binds to and protects mitochondrial DNA and function from damage. *Arterioscler. Thromb. Vasc. Biol.* **29**, 929-935. doi:10.1161/ATVBAHA.109.185546
- Hartmann, C., Hentschel, B., Tatagiba, M., Schramm, J., Schnell, O., Seidel, C., Stein, R., Reifemberger, G., Pietsch, T., Von Deimling, A. et al. (2011). Molecular markers in low-grade gliomas: predictive or prognostic? *Clin. Cancer Res.* **17**, 4588-4599. doi:10.1158/1078-0432.CCR-10-3194
- Hu, W., Ma, S. L., Liu, L. L., Zhu, Y. H., Zeng, T. T., Li, Y. and Guan, X. Y. (2020). Impact of mitochondrial transcription factor A expression on the outcomes of ovarian, endometrial and cervical cancers. *Am. J. Transl. Res.* **12**, 5343-5361.
- Imoto, M., Tachibana, I. and Urrutia, R. (1998). Identification and functional characterization of a novel human protein highly related to the yeast dynamin-like GTPase Vps1p. *J. Cell Sci.* **111**, 1341-1349.
- Ishihara, N., Eura, Y. and Mihara, K. (2004). Mitofusin 1 and 2 play distinct roles in mitochondrial fusion reactions via GTPase activity. *J. Cell Sci.* **117**, 6535-6546. doi:10.1242/jcs.01565
- Khurshed, M., Aarnoudse, N., Hulsbos, R., Hira, V. V. V., Van Laarhoven, H. W. M., Wilmsink, J. W., Molenaar, R. J. and Van Noorden, C. J. F. (2018). IDH1-mutant cancer cells are sensitive to cisplatin and an IDH1-mutant inhibitor counteracts this sensitivity. *FASEB J.* **32**, fj201800547R.
- Konsavage, W. M., Jr, Kyler, S. L., Rennoll, S. A., Jin, G. and Yochum, G. S. (2012). Wnt/beta-catenin signaling regulates Yes-associated protein (YAP) gene

- expression in colorectal carcinoma cells. *J. Biol. Chem.* **287**, 11730-11739. doi:10.1074/jbc.M111.327767
- Lee, Y., Koh, J., Kim, S. I., Won, J. K., Park, C. K., Choi, S. H. and Park, S. H. (2017). The frequency and prognostic effect of TERT promoter mutation in diffuse gliomas. *Acta Neuropathol Commun* **5**, 62. doi:10.1186/s40478-017-0465-1
- Li, F., He, X., Ye, D., Lin, Y., Yu, H., Yao, C., Huang, L., Zhang, J., Wang, F., Xu, S. et al. (2015). NADP(+)-IDH Mutations promote hypersuccinylation that impairs mitochondria respiration and induces apoptosis resistance. *Mol. Cell* **60**, 661-675. doi:10.1016/j.molcel.2015.10.017
- Lin, L., Sabnis, A. J., Chan, E., Olivas, V., Cade, L., Pazarentzos, E., Asthana, S., Neel, D., Yan, J. J., Lu, X. et al. (2015). The Hippo effector YAP promotes resistance to RAF- and MEK-targeted cancer therapies. *Nat. Genet.* **47**, 250-256. doi:10.1038/ng.3218
- Liu-Chittenden, Y., Huang, B., Shim, J. S., Chen, Q., Lee, S. J., Anders, R. A., Liu, J. O. and Pan, D. (2012). Genetic and pharmacological disruption of the TEAD-YAP complex suppresses the oncogenic activity of YAP. *Genes Dev.* **26**, 1300-1305. doi:10.1101/gad.192856.112
- Mammoto, A., Muyleart, M., Kadlec, A., Gutterman, D. and Mammoto, T. (2018). YAP1-TEAD1 signaling controls angiogenesis and mitochondrial biogenesis through PGC1alpha. *Microvasc. Res.* **119**, 73-83. doi:10.1016/j.mvr.2018.04.003
- Massard, C., Zermati, Y., Pauleau, A. L., Larochette, N., Metivier, D., Sabatier, L., Kroemer, G. and Soria, J. C. (2006). hTERT: a novel endogenous inhibitor of the mitochondrial cell death pathway. *Oncogene* **25**, 4505-4514. doi:10.1038/sj.onc.1209487
- Mei, H., Sun, S., Bai, Y., Chen, Y., Chai, R. and Li, H. (2015). Reduced mtDNA copy number increases the sensitivity of tumor cells to chemotherapeutic drugs. *Cell Death Dis.* **6**, e1710. doi:10.1038/cddis.2015.78
- Miwa, S., Czapiewski, R., Wan, T., Bell, A., Hill, K. N., Von Zglinicki, T. and Saretzki, G. (2016). Decreased mTOR signalling reduces mitochondrial ROS in brain via accumulation of the telomerase protein TERT within mitochondria. *Aging (Albany NY)* **8**, 2551-2567. doi:10.18632/aging.101089
- Molenaar, R. J., Botman, R., Smits, M. A., Hira, V. V., Van Lith, S. A., Stap, J., Henneman, P., Khurshed, M., Lenting, K., Mul, A. N. et al. (2015). Radioprotection of IDH1-Mutated Cancer Cells by the IDH1-Mutant Inhibitor AGI-5198. *Cancer Res.* **75**, 4790-4802. doi:10.1158/0008-5472.CAN-14-3603
- Nagaraj, R., Gururaja-Rao, S., Jones, K. T., Slatery, M., Negre, N., Braas, D., Christofk, H., White, K. P., Mann, R. and Banerjee, U. (2012). Control of mitochondrial structure and function by the Yorkie/YAP oncogenic pathway. *Genes Dev.* **26**, 2027-2037. doi:10.1101/gad.183061.111
- Orr, B. A., Bai, H., Oda, Y., Jain, D., Anders, R. A. and Eberhart, C. G. (2011). Yes-associated protein 1 is widely expressed in human brain tumors and promotes glioblastoma growth. *J. Neuropathol. Exp. Neurol.* **70**, 568-577. doi:10.1097/NEN.0b013e31821ff8d8
- Ouyang, T., Meng, W., Li, M., Hong, T. and Zhang, N. (2020). Recent advances of the hippo/YAP signaling pathway in brain development and glioma. *Cell. Mol. Neurobiol.* **40**, 495-510. doi:10.1007/s10571-019-00762-9
- Parsons, D. W., Jones, S., Zhang, X., Lin, J. C., Leary, R. J., Angenendt, P., Mankoo, P., Carter, H., Siu, I. M., Gallia, G. L. et al. (2008). An integrated genomic analysis of human glioblastoma multiforme. *Science* **321**, 1807-1812. doi:10.1126/science.1164382
- Picca, A. and Lezza, A. M. (2015). Regulation of mitochondrial biogenesis through TFAM-mitochondrial DNA interactions: useful insights from aging and calorie restriction studies. *Mitochondrion* **25**, 67-75. doi:10.1016/j.mito.2015.10.001
- Qian, W., Kumar, N., Roginskaya, V., Fouquerel, E., Opresko, P. L., Shiva, S., Watkins, S. C., Kolodiezny, D., Bruchez, M. P. and Van Houten, B. (2019). Chemoptogenetic damage to mitochondria causes rapid telomere dysfunction. *Proc. Natl. Acad. Sci. U.S.A.* **116**, 18435-18444. doi:10.1073/pnas.1910574116
- Rooney, J. P., Ryde, I. T., Sanders, L. H., Howlett, E. H., Colton, M. D., Germ, K. E., Mayer, G. D., Greenamyre, J. T. and Meyer, J. N. (2015). PCR based determination of mitochondrial DNA copy number in multiple species. *Methods Mol. Biol.* **1241**, 23-38. doi:10.1007/978-1-4939-1875-1_3
- Rozengurt, E., Sinnett-Smith, J. and Eibl, G. (2018). Yes-associated protein (YAP) in pancreatic cancer: at the epicenter of a targetable signaling network associated with patient survival. *Signal Transduct Target Ther* **3**, 11. doi:10.1038/s41392-017-0005-2
- Sahin, E., Colla, S., Liesa, M., Moslehi, J., Muller, F. L., Guo, M., Cooper, M., Kotton, D., Fabian, A. J., Walkey, C. et al. (2011). Telomere dysfunction induces metabolic and mitochondrial compromise. *Nature* **470**, 359-365. doi:10.1038/nature09787
- Saunders, J. T., Holmes, B., Benavides-Serrato, A., Kumar, S., Nishimura, R. N. and Gera, J. (2021). Targeting the YAP-TEAD interaction interface for therapeutic intervention in glioblastoma. *J. Neurooncol.* **152**, 217-231.
- Sharma, V., Joseph, C., Ghosh, S., Agarwal, A., Mishra, M. K. and Sen, E. (2007). Kaempferol induces apoptosis in glioblastoma cells through oxidative stress. *Mol. Cancer Ther.* **6**, 2544-2553. doi:10.1158/1535-7163.MCT-06-0788
- Sheikh, I., Gupta, P., Gowda, P., Patrick, S. and Sen, E. (2018). Hexokinase 2 and nuclear factor erythroid 2-related factor 2 transcriptionally coactivate xanthine oxidoreductase expression in stressed glioma cells. *J. Biol. Chem.* **293**, 4767-4777. doi:10.1074/jbc.M117.816785
- Shi, J., Sun, B., Shi, W., Zuo, H., Cui, D., Ni, L. and Chen, J. (2015). Decreasing GSH and increasing ROS in chemosensitivity gliomas with IDH1 mutation. *Tumour Biol.* **36**, 655-662. doi:10.1007/s13277-014-2644-z
- Stein, C., Bardet, A. F., Roma, G., Bergling, S., Clay, I., Ruchti, A., Agarinis, C., Schmelzle, T., Bouwmeester, T., Schubeler, D. et al. (2015). YAP1 Exerts its transcriptional control via TEAD-mediated activation of enhancers. *PLoS Genet.* **11**, e1005465. doi:10.1371/journal.pgen.1005465
- Varghese, F., Bukhari, A. B., Malhotra, R. and De, A. (2014). IHC Profiler: an open source plugin for the quantitative evaluation and automated scoring of immunohistochemistry images of human tissue samples. *PLoS ONE* **9**, e96801. doi:10.1371/journal.pone.0096801
- Wallace, D. C. (2012). Mitochondria and cancer. *Nat. Rev. Cancer* **12**, 685-698. doi:10.1038/nrc3365
- Wei, S., Wang, J., Oyindade, O., Ma, D., Wang, S., Kratz, L., Lal, B., Xu, Q., Liu, S., Shah, S. R. et al. (2018). Heterozygous IDH1(R132H/WT) created by "single base editing" inhibits human astroglial cell growth by downregulating YAP. *Oncogene* **37**, 5160-5174. doi:10.1038/s41388-018-0334-9
- Woo, D. K., Green, P. D., Santos, J. H., D'souza, A. D., Walther, Z., Martin, W. D., Christian, B. E., Chandel, N. S. and Shadel, G. S. (2012). Mitochondrial genome instability and ROS enhance intestinal tumorigenesis in APC(Min/+) mice. *Am. J. Pathol.* **180**, 24-31. doi:10.1016/j.ajpath.2011.10.003
- Zhang, J., Wong, C. C., Leung, K. T., Wu, F., Zhou, Y., Tong, J. H. M., Chan, R. C. K., Li, H., Wang, Y., Yan, H. et al. (2020a). FGF18-FGFR2 signaling triggers the activation of c-Jun-YAP1 axis to promote carcinogenesis in a subgroup of gastric cancer patients and indicates translational potential. *Oncogene* **39**, 6647-6663. doi:10.1038/s41388-020-01458-x
- Zhang, Q., Liu, N., Bai, J., Zhou, Q., Mao, J., Xu, L., Liu, J., Wei, H., Ren, C., Wu, X. et al. (2020b). Human telomerase reverse transcriptase is a novel target of Hippo-YAP pathway. *FASEB J.* **34**, 4178-4188. doi:10.1096/fj.201902147R
- Zhao, B., Ye, X., Yu, J., Li, L., Li, W., Li, S., Yu, J., Lin, J. D., Wang, C. Y., Chinnaiyan, A. M. et al. (2008). TEAD mediates YAP-dependent gene induction and growth control. *Genes Dev.* **22**, 1962-1971. doi:10.1101/gad.1664408
- Zhao, B., Li, L., Lei, Q. and Guan, K. L. (2010). The Hippo-YAP pathway in organ size control and tumorigenesis: an updated version. *Genes Dev.* **24**, 862-874.

Supplementary Figure S1

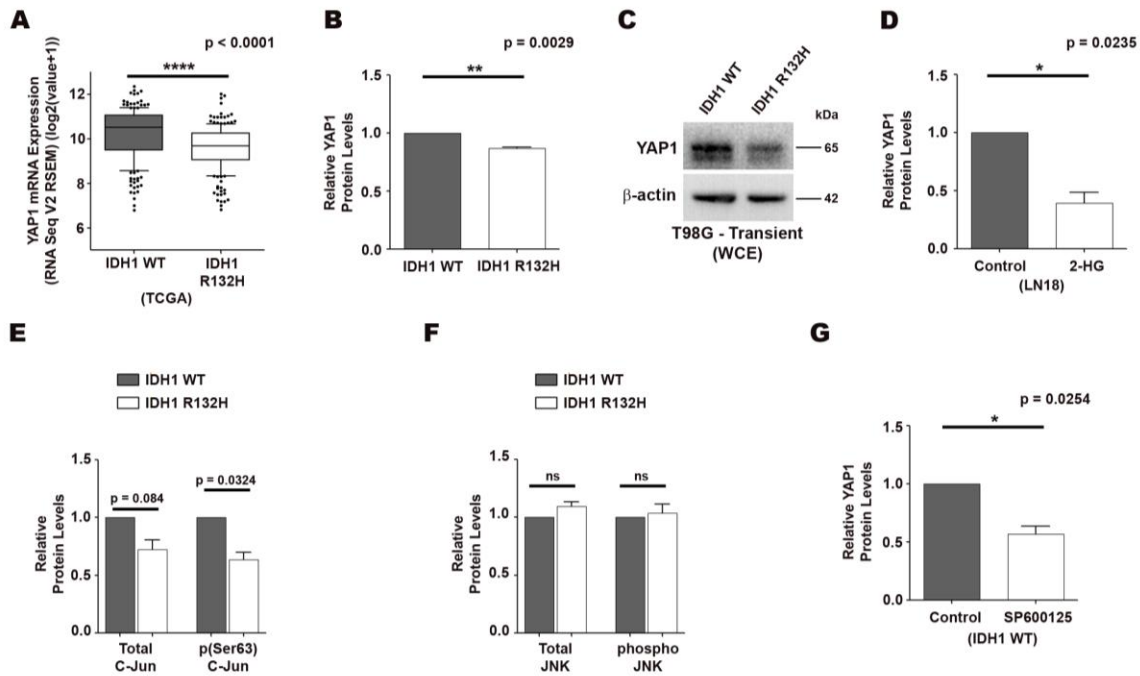


Fig. S1. Reduced YAP1 and C-Jun levels in IDH1 R132H and 2-HG-treated cells

- RNA expression data from TCGA shows lower YAP1 expression in IDH1 R132H gliomas as compared to IDH1 WT gliomas. Data from N=204 IDH1 WT and 206 IDH1 R132H patients from TCGA have been used for analysis. Whiskers represent 10-90 percentile. *****, $p < 0.0001$ (Two-tailed student's t-test)
- Densitometric analysis of immunoblots shows lower YAP1 protein levels in IDH1 R132H as compared to IDH1 WT cells
- Immunoblots show a decrease in YAP1 levels in T98G cells transiently transfected with IDH1 R132H. The blots are representative of two independent experiments with similar results. WCE, whole cell extract
- Densitometric analysis of immunoblots shows a reduction in YAP1 protein levels in LN18 cells upon 2-HG treatment

- E. Densitometric analysis of immunoblots shows a reduction in total and phosphorylated (Ser63) C-Jun protein levels in IDH1 R132H cells
- F. Densitometric analysis of immunoblots shows no difference in total and phosphorylated JNK protein levels between IDH1 WT and IDH1 R132H cells
- G. Densitometric analysis of immunoblots shows a reduction in YAP1 protein levels on treatment of IDH1 WT cells with SP600125

All densitometry graphs represent data expressed as fold change over respective controls, presented as mean \pm SEM. N=3 biological replicates. *, $p<0.05$; **, $p<0.01$. Paired two-tailed student's t-test were used for statistical analysis

Supplementary Figure S2

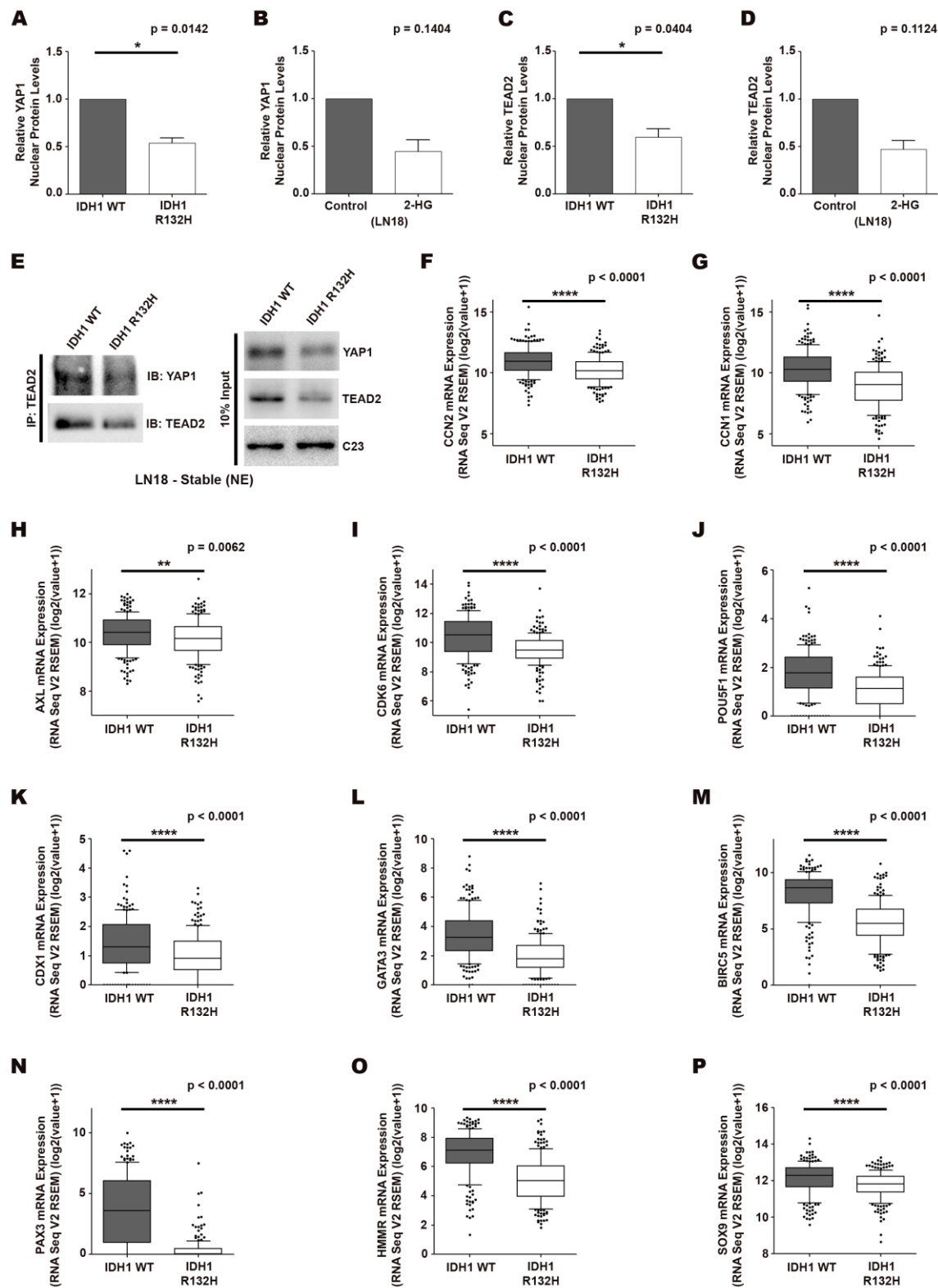


Fig. S2. Reduced Nuclear YAP1 and TEAD2 levels and diminished YAP1/TEAD activity in IDH1 R132H

- A. Densitometric analysis shows diminished nuclear YAP1 levels in IDH1 R132H as compared to IDH1 WT cells
- B. Densitometric analysis shows a reduction in nuclear YAP1 levels in 2-HG-treated LN18 cells
- C. Densitometry shows diminished nuclear TEAD2 levels in IDH1 R132H as compared to IDH1 WT cells
- D. Densitometric analysis shows a reduction in nuclear TEAD2 levels upon 2-HG treatment in LN18 cells
- E. Coimmunoprecipitation (CoIP) demonstrates reduced YAP1/TEAD2 complex formation in IDH1 R132H cells. The blots are representative of two independent experiments with similar results.
NE, nuclear extract
- F-P. TCGA data analysis shows lower expression of known TEAD-responsive genes in IDH1 R132H gliomas as compared to IDH1 WT gliomas. Data from N=204 IDH1 WT and 206 IDH1 R132H patients have been used for the analysis. Whiskers represent 10-90 percentile. **, $p < 0.01$; ****, $p < 0.0001$ (Two-tailed student's t-test)

All densitometry graphs represent data expressed as fold change over respective controls, presented as mean \pm SEM. N=3 biological replicates (N=2 biological replicates for nuclear protein levels in 2-HG-treated cells). *, $p < 0.05$. Paired two-tailed student's t-test was used for statistical analysis

Supplementary Figure S3

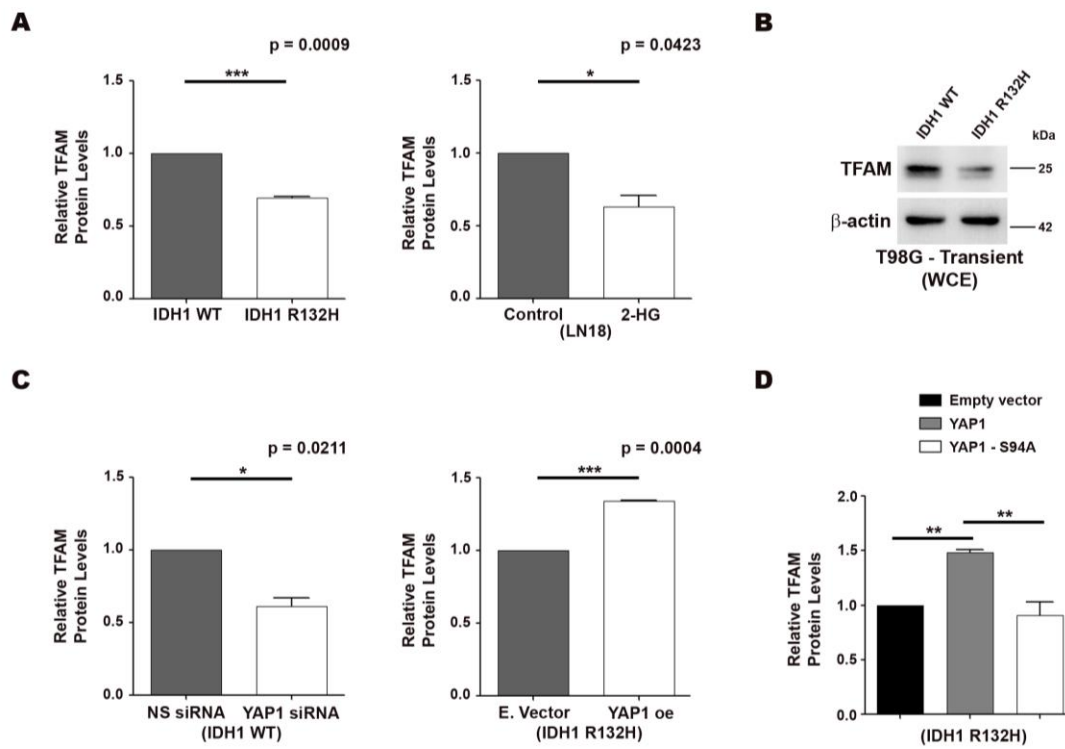


Fig. S3. YAP1-dependent TFAM levels

- Densitometric analysis of immunoblots shows lower TFAM protein levels in IDH1 R132H cells and 2-HG-treated LN18 cells as compared to IDH1 WT and control cells respectively
- Immunoblots show a decrease in TFAM levels in T98G cells transiently transfected with IDH1 R132H. The blots are representative of two independent experiments with similar results. WCE, whole cell extract
- Densitometric analysis shows a reduction in TFAM levels upon siRNA-mediated knockdown of YAP1 in IDH1 WT cells, and an increase in TFAM levels on overexpressing YAP1 in IDH1 R132H cells
- Densitometric analysis shows an increase in TFAM levels on overexpressing wild type YAP1 in IDH1 R132H cells, but not on overexpressing YAP1-S94A mutant.

All densitometry graphs represent data expressed as fold change over respective controls, presented as mean \pm SEM. N=3 biological replicates. *, $p < 0.05$; **, $p < 0.01$; ***, $p < 0.001$. Comparisons between two groups were done using paired two-tailed student's t-test, and comparisons among multiple groups were done using one-way ANOVA with Tukey's multiple comparison test. NS siRNA, Non-specific siRNA; E. vector, Empty vector; YAP1 oe, YAP1 overexpression

Supplementary Figure S4

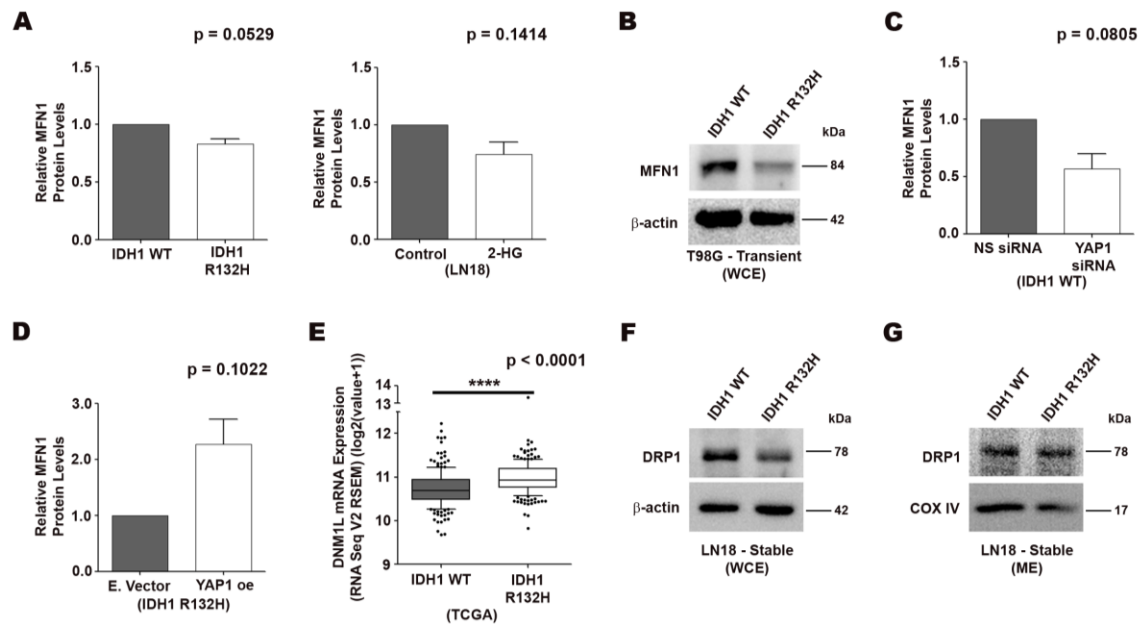


Fig. S4. Altered MFN1 and DRP1 levels in IDH1 R132H cells

- Densitometric analysis shows lower MFN1 protein levels in IDH1 R132H cells and 2-HG-treated LN18 cells
- Immunoblot shows a decrease in MFN1 levels in T98G cells transiently transfected with IDH1 R132H. The blots are representative of two independent experiments with similar results. WCE, whole cell extract
- Densitometry shows a reduction in MFN1 protein levels upon siRNA-mediated knockdown of YAP1 in IDH1 WT cells
- Densitometry shows an increase in MFN1 levels on overexpressing YAP1 in IDH1 R132H cells
- TCGA data analysis shows higher DNM1L (DRP1) expression in IDH1 R132H gliomas as compared to IDH1 WT gliomas. Data from N=204 IDH1 WT and 206 IDH1 R132H patients from TCGA have been used for analysis. Whiskers represent 10-90 percentile. ****, p<0.0001 (Two-tailed student's t-test)

- F. Immunoblots show reduced levels of DRP1 in IDH1 R132H cells. The blots are representative of three independent experiments with similar results.
- G. Immunoblots with mitochondrial protein fractions show higher recruitment of DRP1 in the mitochondria of IDH1 R132H cells as compared to IDH1 WT. The blots are representative of two independent experiments with similar results.

All densitometry graphs represent data expressed as fold change over respective controls, presented as mean \pm SEM. N=3 biological replicates. Paired two-tailed student's t-test was used for statistical analysis. WCE, whole cell extract; ME, mitochondrial extract; NS siRNA, Non-specific siRNA; E. vector, Empty vector; YAP1 oe, YAP1 overexpression

Supplementary Figure S5

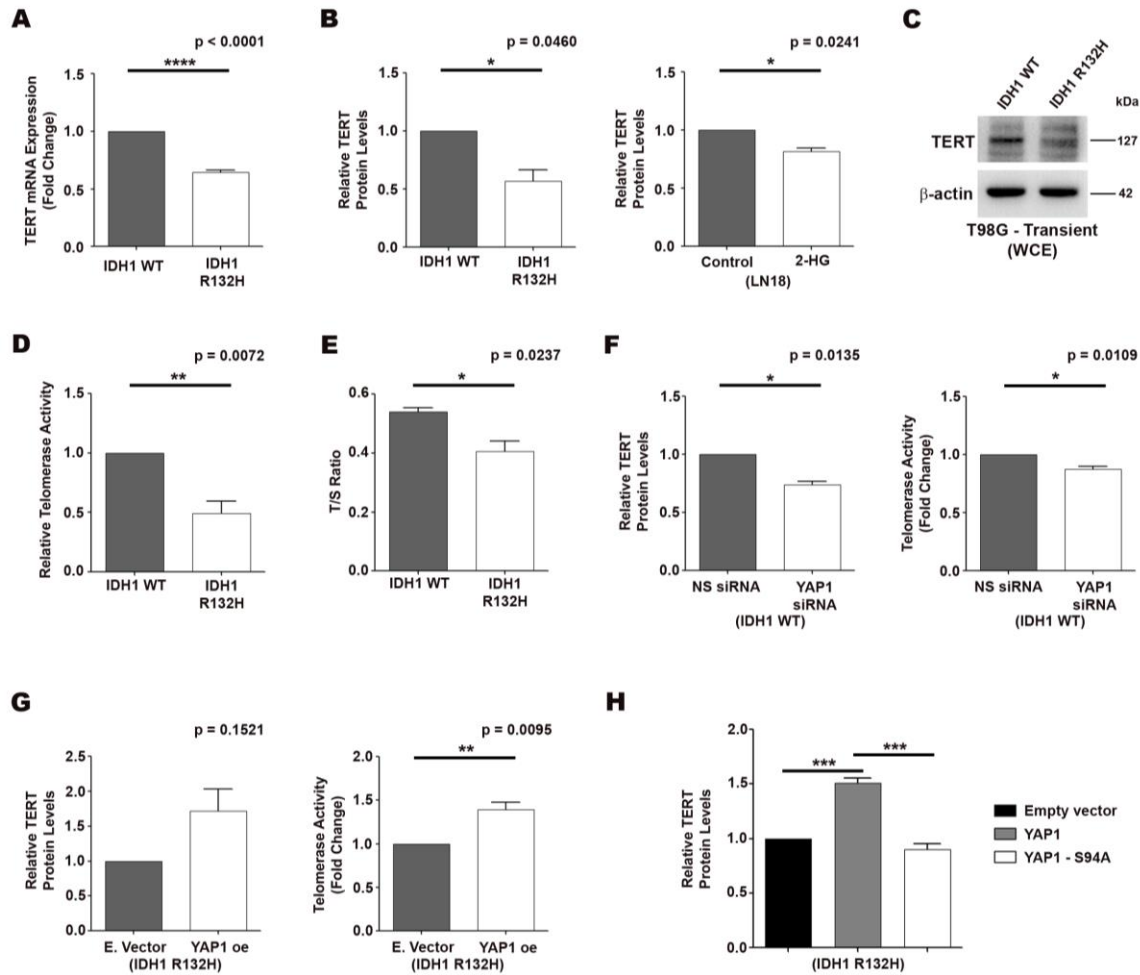


Fig. S5. YAP1-dependent TERT expression and telomerase activity

- qRT-PCR shows reduced TERT mRNA levels in IDH1 R132H cells. Data are expressed as fold change over IDH1 WT and presented as mean \pm SEM. N=5 biological replicates. ****, $p < 0.0001$ (Two-tailed student's t-test)
- Densitometric analysis of immunoblots shows lower TERT protein levels in IDH1 R132H cells and 2-HG-treated LN18 cells as compared to IDH1 WT and control cells respectively
- Immunoblots show a decrease in TERT levels in T98G cells transiently transfected with IDH1 R132H. The blots are representative of two independent experiments with similar results. WCE, whole cell extract
- Telomeric repeat amplification protocol (TRAP) assay shows decreased telomerase activity in IDH1 R132H cells as compared to IDH1 WT. Data are expressed as fold change over IDH1 WT and presented as mean \pm SEM. N=3 biological replicates. **, $p < 0.01$ (Two-tailed student's t-test)

- E. Telomere length measurement by qPCR shows a reduction in IDH1 R132H cells. Data are presented as mean \pm SEM. N=3 biological replicates. T/S ratio, ratio of telomere to single copy gene 36B4; *, $p < 0.05$ (Two-tailed student's t-test)
- F. Densitometry shows a reduction in TERT protein levels upon siRNA-mediated knockdown of YAP1 in IDH1 WT cells. TRAP assay reveals a decrease in telomerase activity on siRNA-mediated knockdown of YAP1 in IDH1 WT cells
- G. Densitometry shows an increase in TERT protein levels upon overexpression of YAP1 in IDH1 R132H cells. TRAP assay reveals an increase in telomerase activity on overexpressing YAP1 in IDH1 R132H cells
- H. Densitometric analysis shows an increase in TERT levels on overexpressing wild type YAP1 in IDH1 R132H cells, but not on overexpressing YAP1-S94A mutant

All densitometry graphs represent data expressed as fold change over respective controls, presented as mean \pm SEM. N=3 biological replicates. *, $p < 0.05$; **, $p < 0.01$; ***, $p < 0.001$. Comparisons between two groups were done using paired two-tailed student's t-test, and comparisons among multiple groups were done using one-way ANOVA with Tukey's multiple comparison test. NS siRNA, Non-specific siRNA; E. vector, Empty vector; YAP1 oe, YAP1 overexpression

Supplementary Figure S6

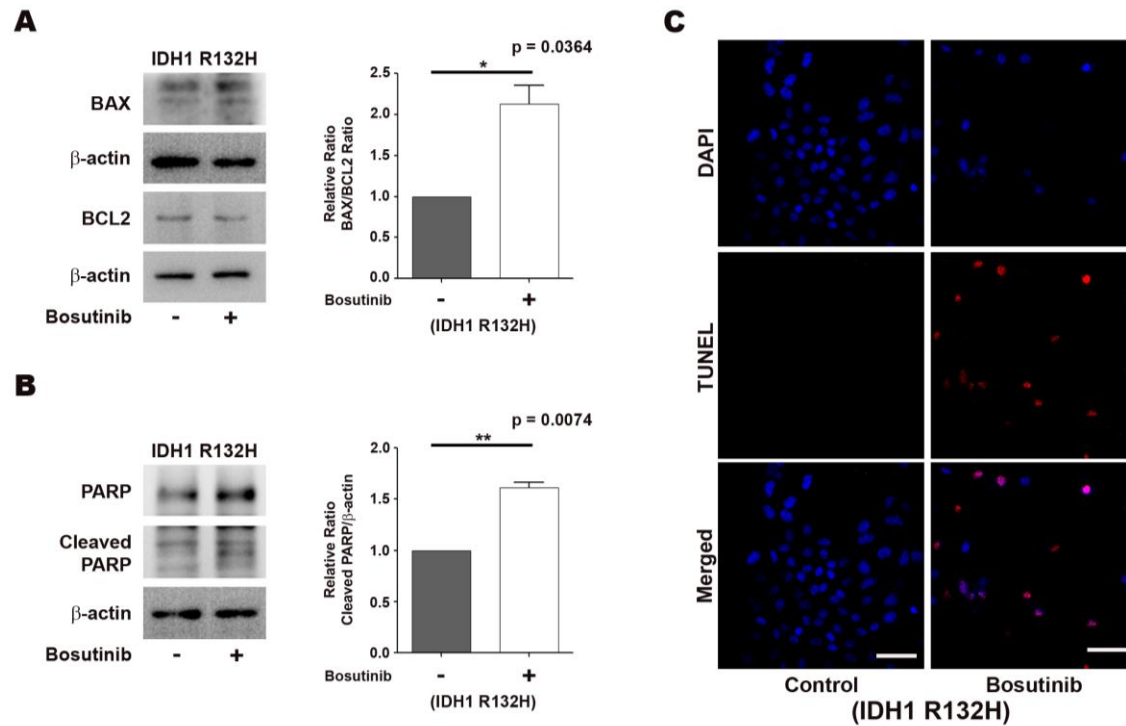


Fig. S6. Apoptosis in IDH1 R132H cells upon Bosutinib treatment

- Immunoblots and densitometric analysis show an increase in BAX/BCL2 ratio in Bosutinib-treated IDH1 R132H cells
- Immunoblots and densitometric analysis show an increase in cleaved PARP levels in Bosutinib-treated IDH1 R132H cells
- Maximum intensity projections of confocal microscopic images of IDH1 R132H cells showing TUNEL staining under control and Bosutinib-treated conditions

Graphs represent data expressed as fold change over control, presented as mean \pm SEM. N=3 biological replicates. *, $p < 0.05$; **, $p < 0.01$ (Paired two-tailed student's t-test)

Supplementary Figure S7

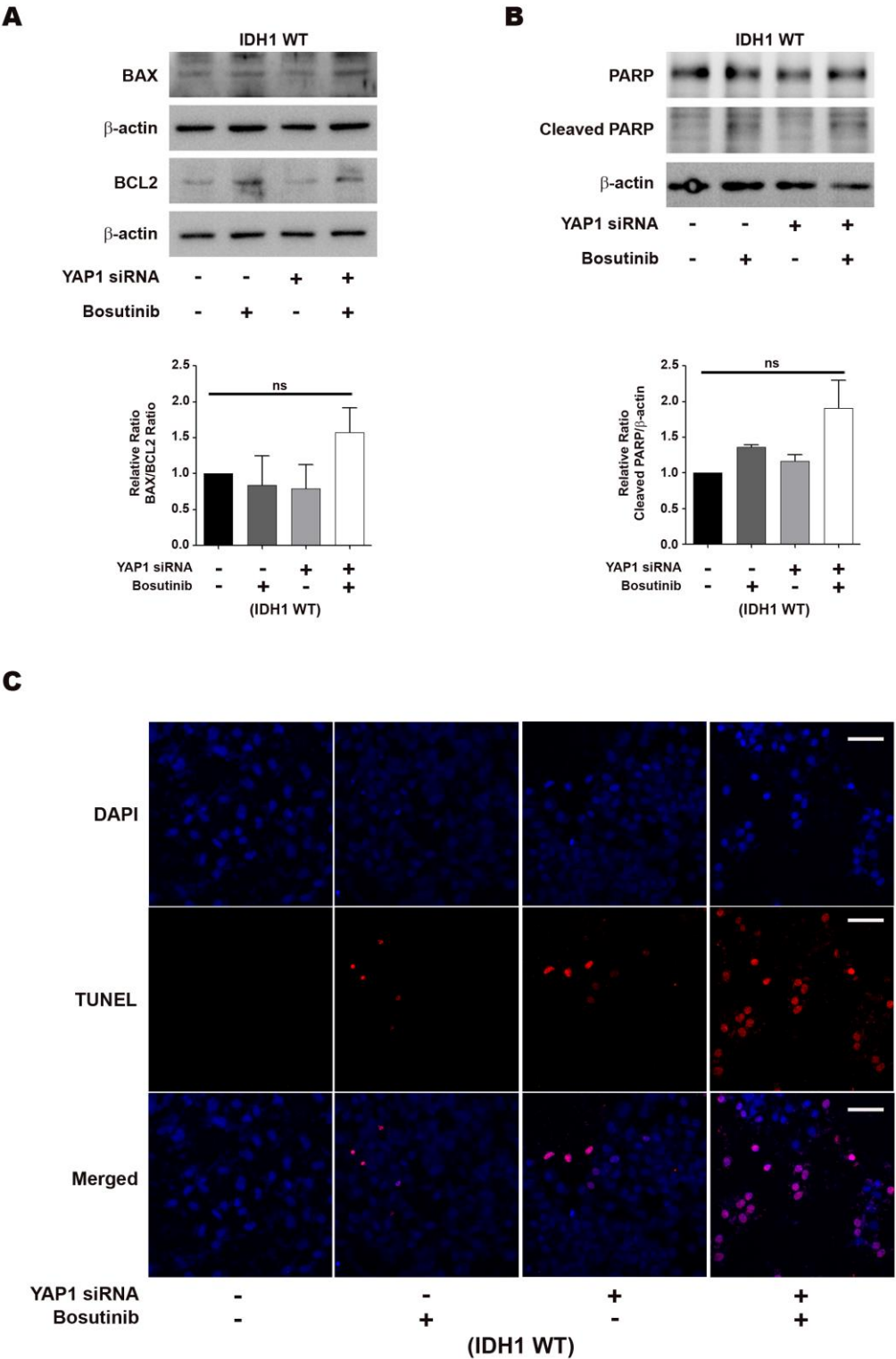


Fig. S7. Apoptosis in IDH1 WT cells upon YAP1 depletion and Bosutinib treatment

- A. Immunoblots and densitometric analysis show an increase in BAX/BCL2 ratio upon Bosutinib treatment along with siRNA-mediated knockdown of YAP1 in IDH1 WT cells
- B. Immunoblots and densitometric analysis show an increase in cleaved PARP levels in IDH1 WT cells on treatment with Bosutinib along with siRNA-mediated knockdown of YAP1.
- C. Maximum intensity projections of confocal microscopic images of IDH1 WT cells showing TUNEL staining under the specified conditions

Graphs represent data expressed as fold change over control, presented as mean \pm SEM. N=3 biological replicates (N=2 for cleaved PARP). ns, not significant (One-way ANOVA with Tukey's multiple comparison test)

Table S1. Sequences of primers used in the study

Gene	Primer Sequences
1. pGL3 TFAM WT (Cloning)	Forward: CGACGCGTTGCTCAAATTAAGCAAGCTG Reverse: GGAAGATCTCGCTCCGGTGGATGAGGCAG
2. pGL3 TFAM Δ (SDM)	Forward: TCCGCCCCGACTGGAGCACATCTACCGACCGGATGT Reverse: CGGTAGATGTGCTCCAGTCGGGGCGGAATTGGCGCA
3. pBABE YAP1 S94A (SDM)	Forward: TGCCCGACGCGTTCTCAAGCCGCCGGA Reverse: TTGAAGAACGCGTCGGGCAGCTTCCGGA
4. <i>YAP1</i>	Forward: GGCGCTCTCAACGCCGTCATGAAC Reverse: CCTGTCGGGAGTGGGATTT
5. <i>TERT</i>	Forward: GGATGAAGCGGAGTCTGGA Reverse: CGGAAGAGTGTCTGGAGCAA
6. <i>TFAM</i> (ChIP)	Forward: ATTGCGGTTTCCCTTCATCT Reverse: GCCACTAGCGAGGCACTATG
7. <i>GAPDH</i> (ChIP)	Forward: TACTAGCGGTTTTACGGGCG Reverse: TCGAACAGGAGGAGCAGAGAGCGA
8. Telomere	Forward: GGTTTTTGAGGGTGAGGGTGAGGGTGAGGGTGAGGGT Reverse: TCCCGACTATCCCTATCCCTATCCCTATCCCTATCCCTA
9. <i>36B4/RPLP0</i>	Forward: CAGCAAGTGGGAAGGTGTAATCC Reverse: CCCATTCTATCATCAACGGGTACAA
10. <i>ND1</i>	Forward: ACGCCATAAACTCTTCACCAAAG Reverse: TAGTAGAAGAGCGATGGTGAGAGCTA
11. <i>B2M</i>	Forward: TGCTGTCTCCATGTTTGATGTATCT Reverse: TCTCTGCTCCCCACCTCTAAGT

SDM, site directed mutagenesis.